# DESIGN AND SIMULATION OF MHz INDUCTIVE OUTPUT TUBE

Professor Yubin Gong

University of Electronic Science and Technology of China

August 26-29, 2026
Bab Honnef, Germany

# This year is the 70th Anniversary of UESTC

# Contents

# 1. Introduction

## X-ray scan（CT)

- Fast inspection speed
- High density resolution
- Clear section relationship

## Magnetic Resonance (MRT)

- High resolution
- Multiple sequence parameters
- Large field of view

## Positron emission (PET)

- High sensitivity
- High image contrast
- Functional dynamic imaging

## Ultrasound

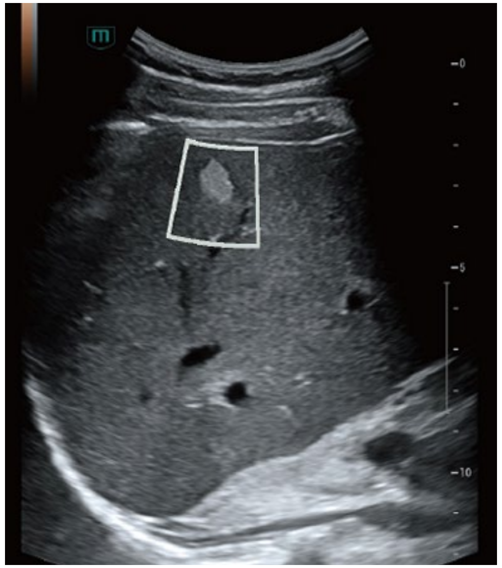

- No ionizing radiation
- Portable and low cost
- Real-time dynamic imaging

**Each existing medical imaging technologies have their own advantages in terms of tissue penetration depth, sensitivity, and specificity. There is an need for a non-invasive/minimally invasive, high-resolution, structural and functional imaging technology that complements the existing technologies and is specifically targeted at deep tissues.**

# 1. Introduction-Microwave Induced Thermoacoustic Imaging

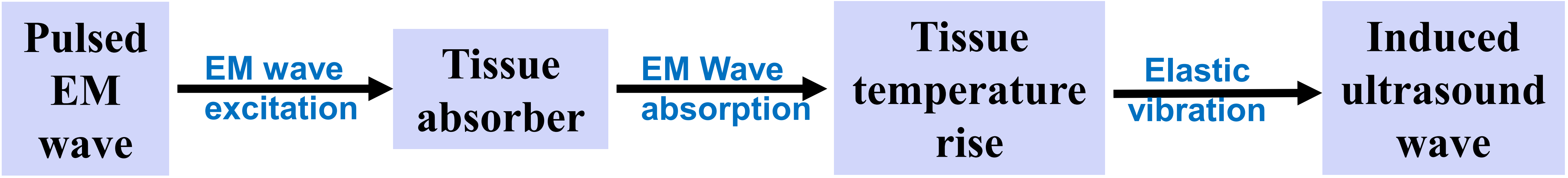


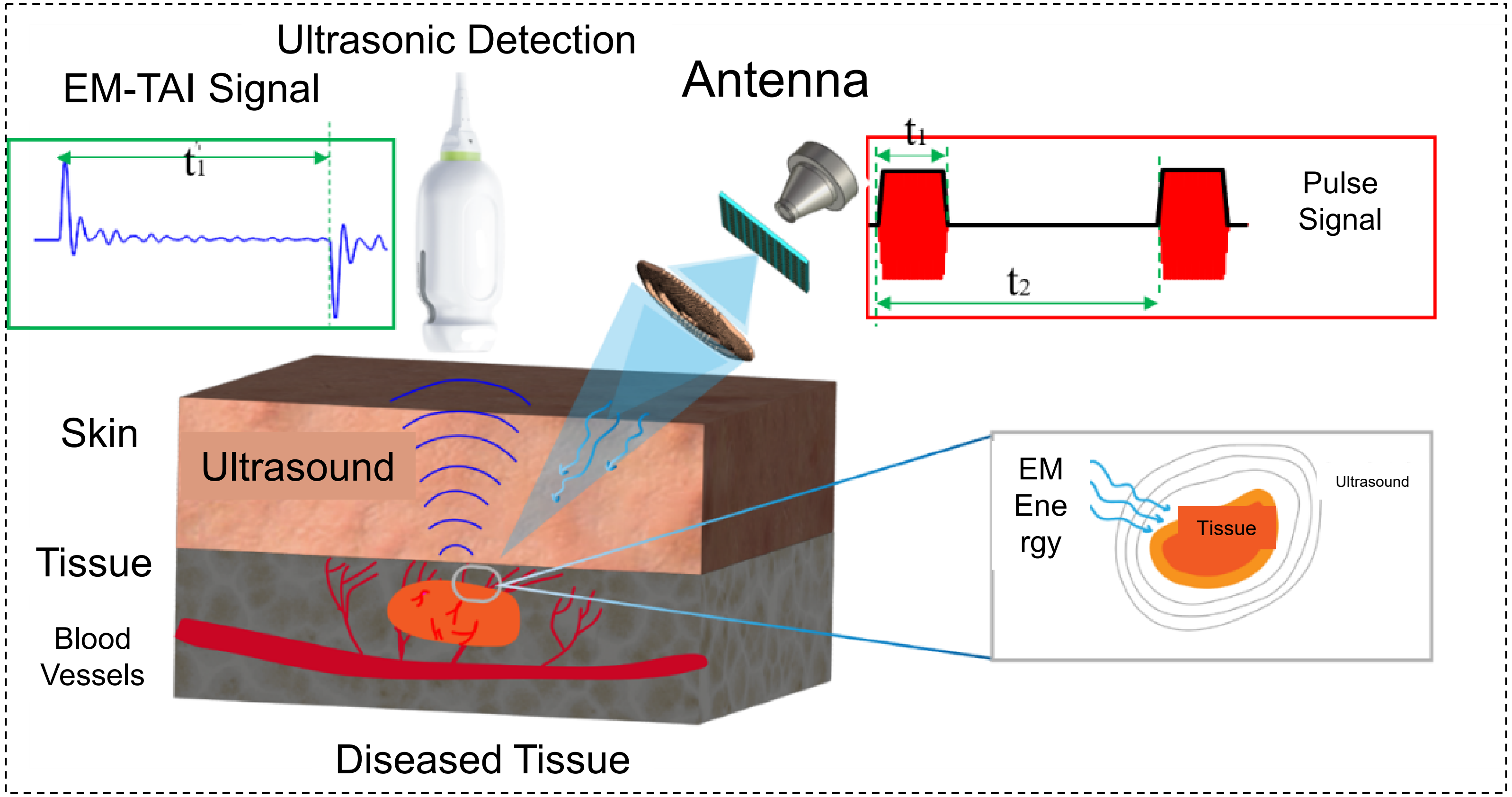


Fig.1.1 Schematic of electromagnetic Wave-induced Thermoacoustic Imaging (EM-TAI)

- Compared to traditional ultrasound, it can not only detect structure abnormalities but also obtain electrical parameters of biological tissues, such as dielectric constant.
- Typically, there is a significant difference in dielectric constants between normal and abnormal tissues.
- Based on this principle, it should have important applications in health examination.

# 1. Introduction

| | | | |
|---|---|---|---|
| Depth of penetration | Requirements for microwave sources → | Low frequency, High power | |
| No cell damage | Requirements for microwave sources → | Small total energy | |

⇒ **Microwave source:**
- Low frequency
- Short pulse
- High peak power

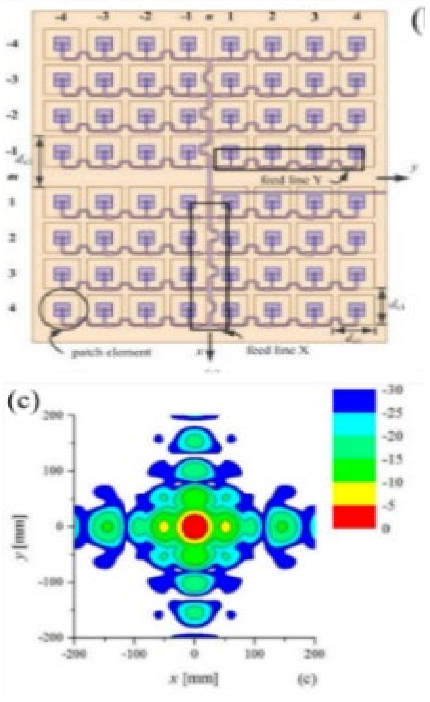


Fig.1.2 Efficient excitation of ultrasonic signal

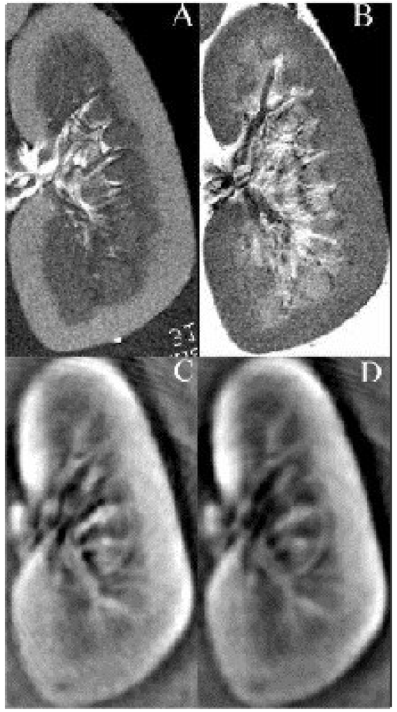


Fig.1.3 Structural and functional imaging

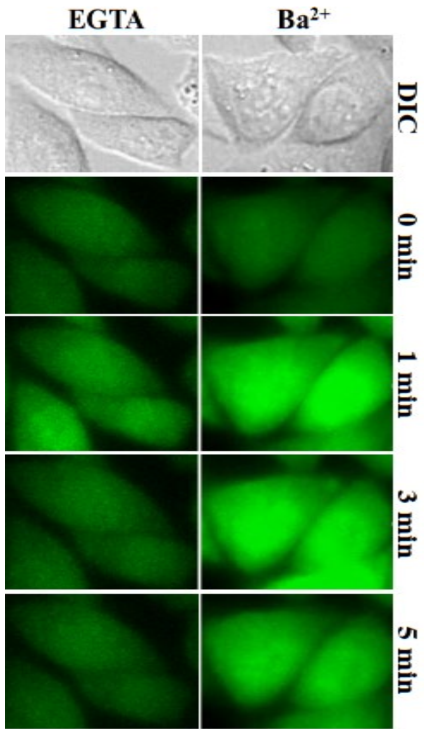


Fig.1.4 Biological effect assessment

# 1. Introduction

- **Biological tissues have a good absorption capacity for microwaves below 1 GHz. Meanwhile, the relatively long wavelength of microwaves below 1 GHz ensures the depth of penetration.**

- **The working frequency band of IOT is precisely below several GHz. It is a miniaturized and highly efficient microwave amplifier. So, it is highly suitable as the microwave source for microwave thermoacoustic imaging.**

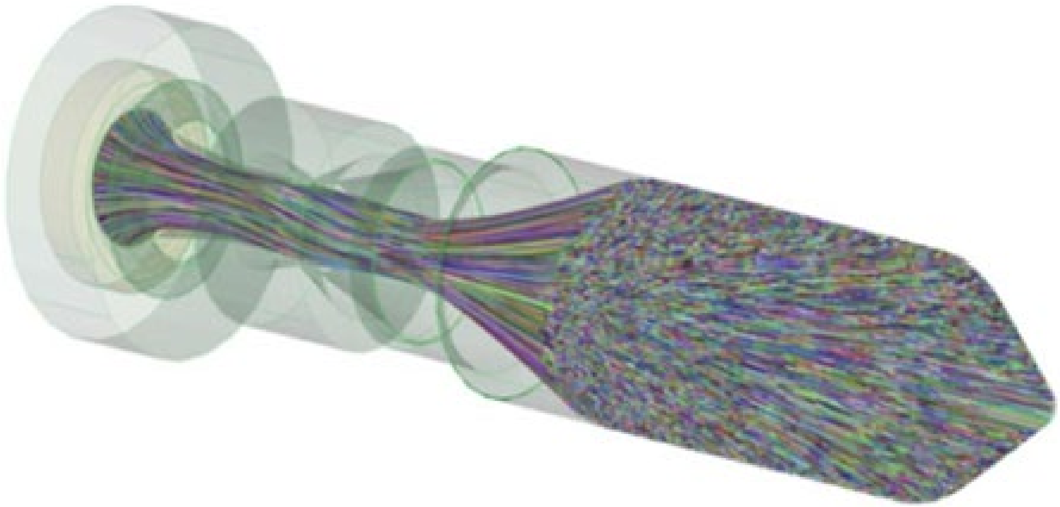

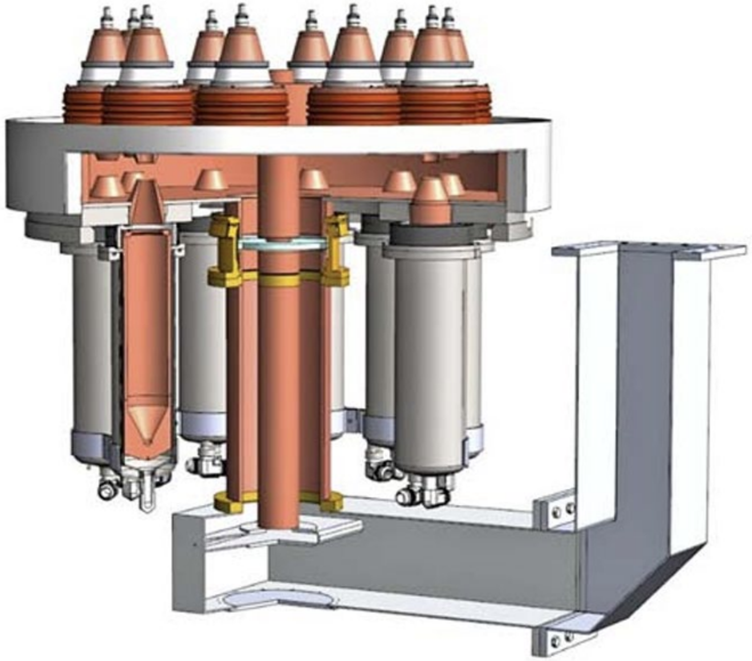

# 1. Introduction

- **IOT was invented by Haeff at the same time as klystron. However, the klystron has a higher gain.**
- **Meanwhile, the grid processing and heat resistance issues of IOT have led to a stagnation in the research and optimization of IOT.**
- **It was not until the 1980s that IOT was re-examined due to the advancement of processing technology and the demand for the development of small-sized and high efficient microwave sources.**

Andrew V. Haeff

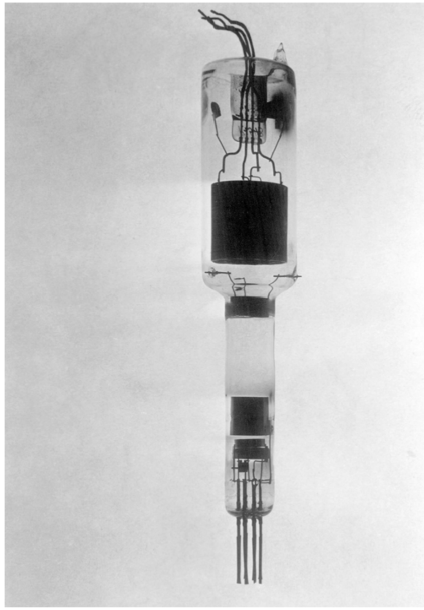

Haeff's prototype tube

| Parameters | 250 kW CW klystrode (Los Alamos)[5] | 10TD2130 (E2V)[6] | VKP-9050 IOT Amplifier (CPI) | VKP-9130 IOT Amplifier (CPI) | 100 kW CW Multi-beam Klystrode[7] |
|---|---|---|---|---|---|
| Frequency (MHz) | 267 | 470–810 | 500 | 1300 | 1300 |
| Output power (kW) | 250 CW | 80–60 | 90 CW | 30 CW or 90 pulsed | 100 CW |
| Beam voltage (kV) | 65 | 36–38 | 40 | 35/42 | 24 |
| Beam current (A) | 5.5 | 2.2–1.57 | 3.5 | 1.3/3.4 | 4 |
| Efficiency (%) | >70 | 65–58 | >65% | >60% | ≅ 80 |
| Operating regime | Class B | Class B | Class B | Class B | Class C |

# 1. Introduction

- **The function of the IOT input cavity is to couple microwave energy to the area between the cathode and the grid.**
- **The cathode emits pre-modulated electron beams under the combined action of direct current voltage and radio frequency voltage.**
- **The electron can complete the beam-wave interaction simply by passing through the gap of the output cavity.**
- **Since there is no need for drift clustering, the volume of IOT is much smaller than that of the speed modulator device.**

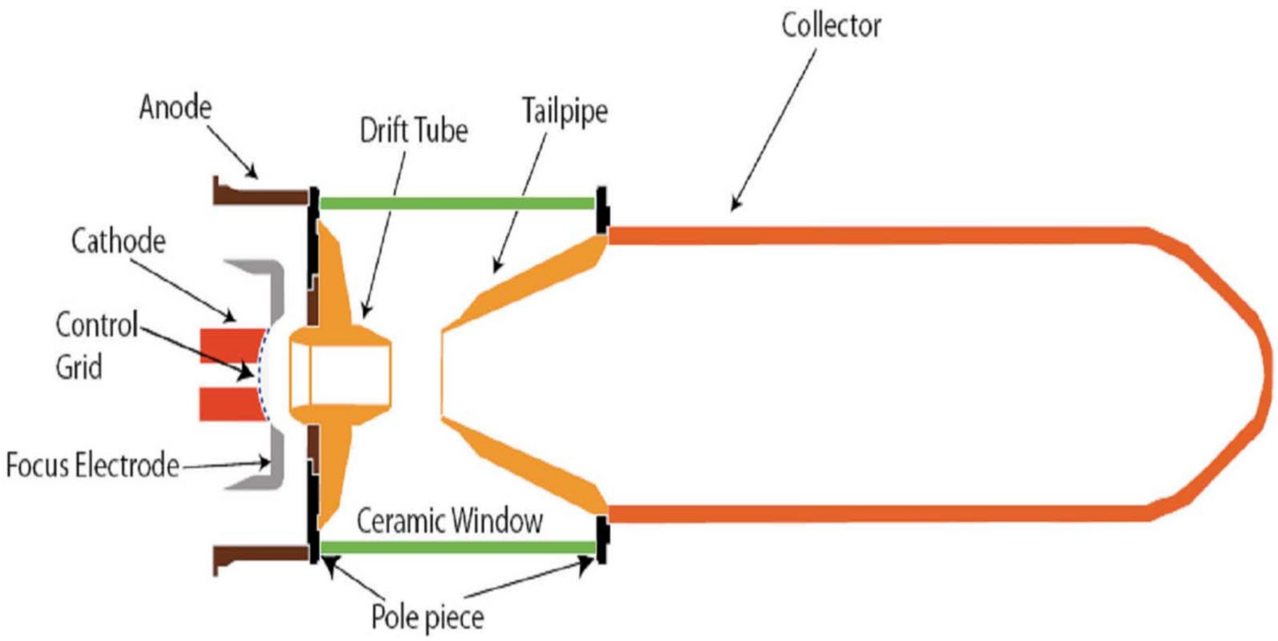


Fig.2.1 Schematic illustration of an inductive output tube[1]

# 1. Introduction-Structure and simulation methods of IOT

**EM Wave** —Coupling→ **Input Cavity** —Resonance→ **RF Voltage** —Modulation→ **Electron Emission**

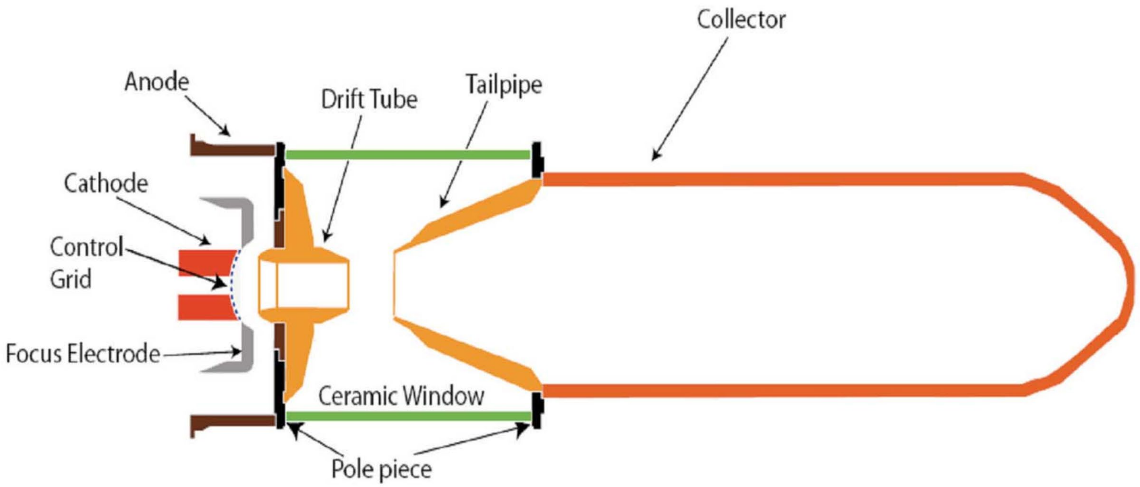


Fig.2.1 Schematic illustration of an inductive output tube[1]

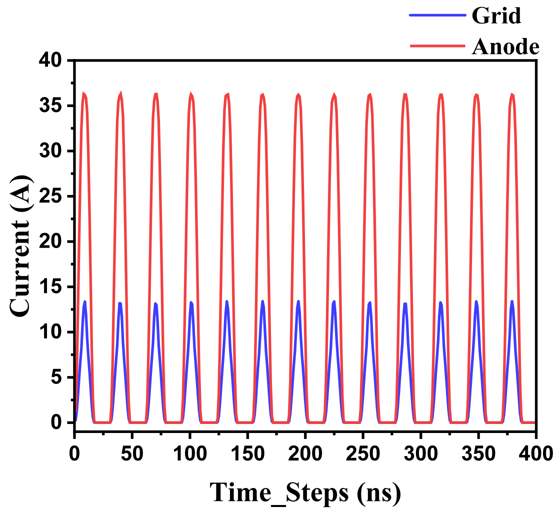


Fig.2.2 Input cavity emission current

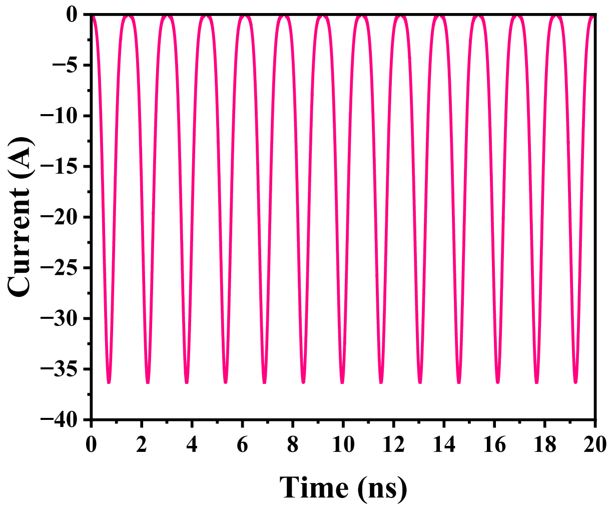


Fig.2.3 Beam-wave interaction current


[1] H. P. Freund, W. H. Miner, J. Verboncoeur, Y. Li and E. Wright, "Time-Domain Simulation of Inductive Output Tubes," in IEEE Transactions on Plasma Science, vol. 35, no. 4, pp. 1081-1088, Aug. 2007, doi: 10.1109/TPS.2007.902137.

# Contents

## (2.1.1) Model of Input cavity for 434 MHz IOT

**The model of input cavity for 434 MHz IOT with spherical grid and spherical cathode can be simplified to a quarter-wavelength coaxial resonator consisting of two isolated media.**

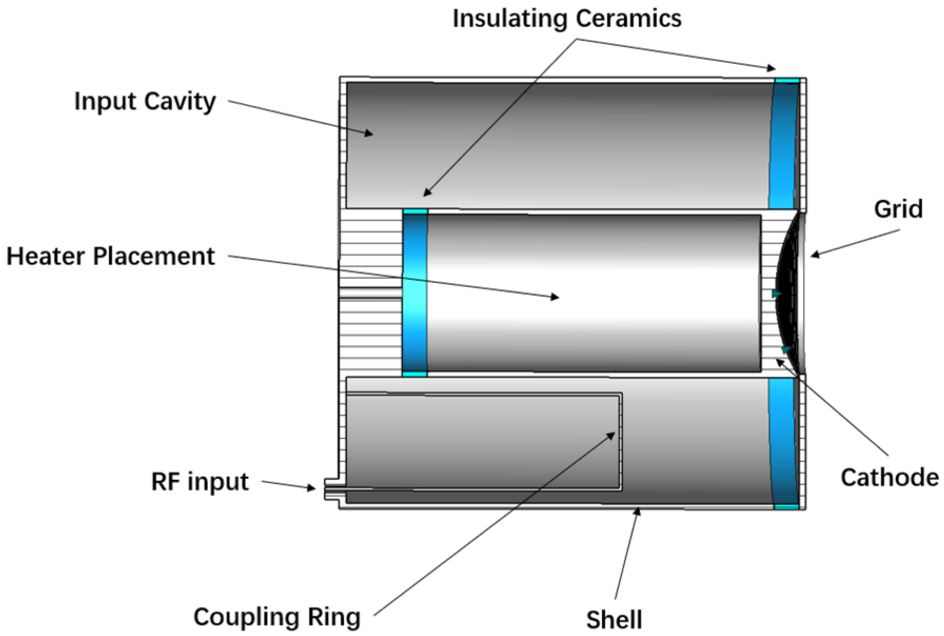


Fig.3.1 Cross-section view of the input cavity

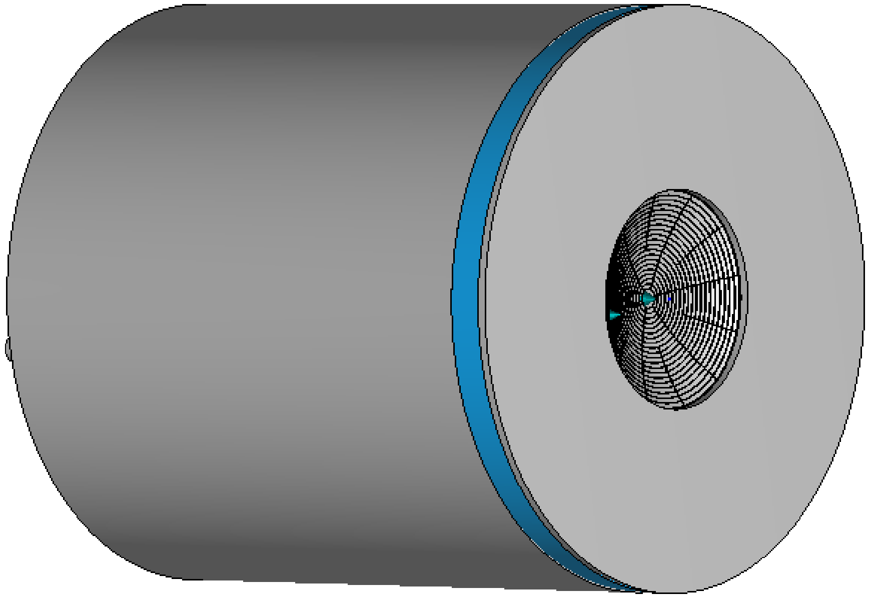

Fig.3.2 Model of the spherical grid input cavity

## (2.1.2) Electromagnetic simulation of Input cavity for 434 MHz IOT

**The standing wave electric field of the input cavity is mainly concentrated between the cathode and the grid, while the magnetic field is very small in the cathode and grid regions.**

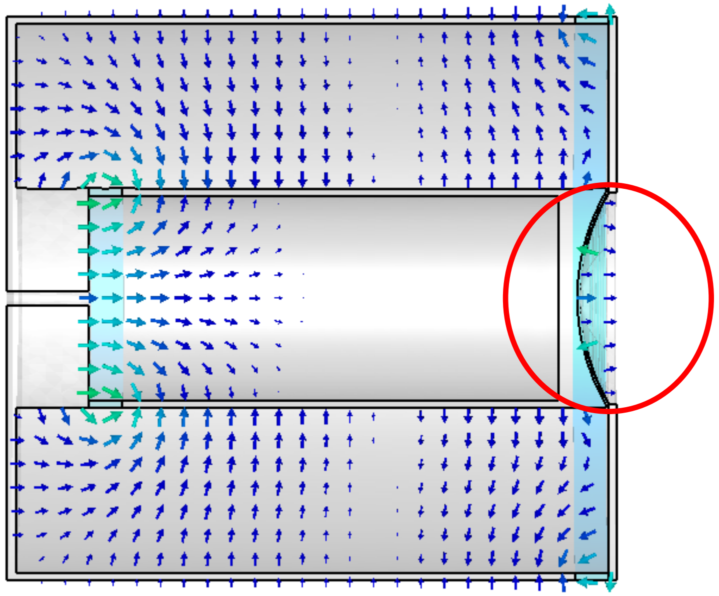

Fig.3.3 RF electric field distribution of the input cavity

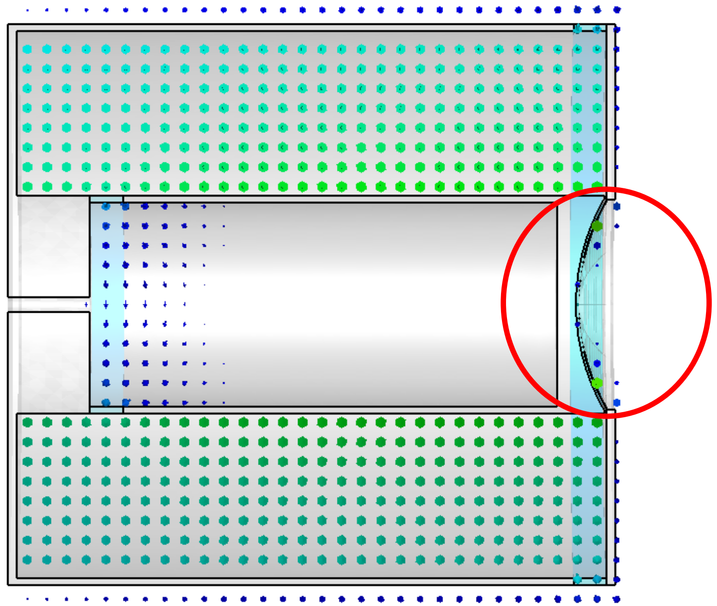

Fig.3.4 RF magnetic field distribution of the input cavity

## (2.1.2) Electromagnetic simulation of Input cavity for 434 MHz IOT

**Time domain Solver of CST Studio Suite was used for simulation to obtain the reflection coefficient of the input cavity and the RF voltage between the cathode and the grid.**

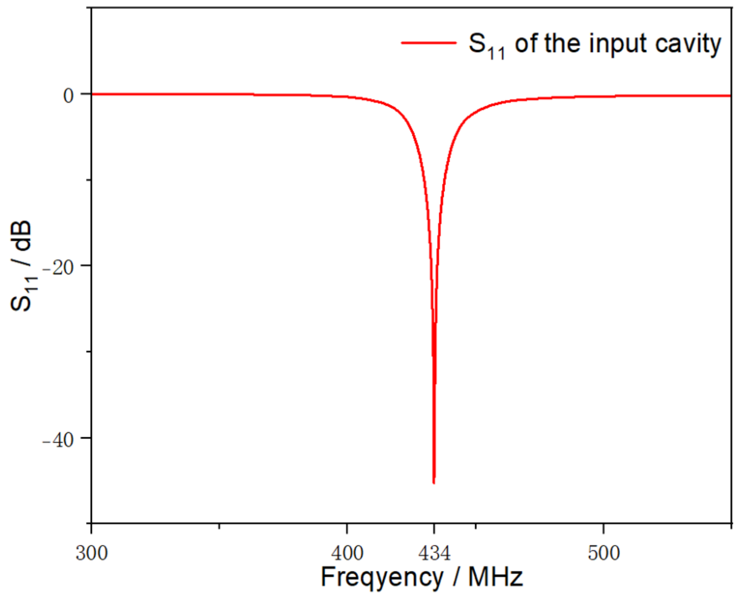


Fig.3.5 Reflection coefficient of the input cavity

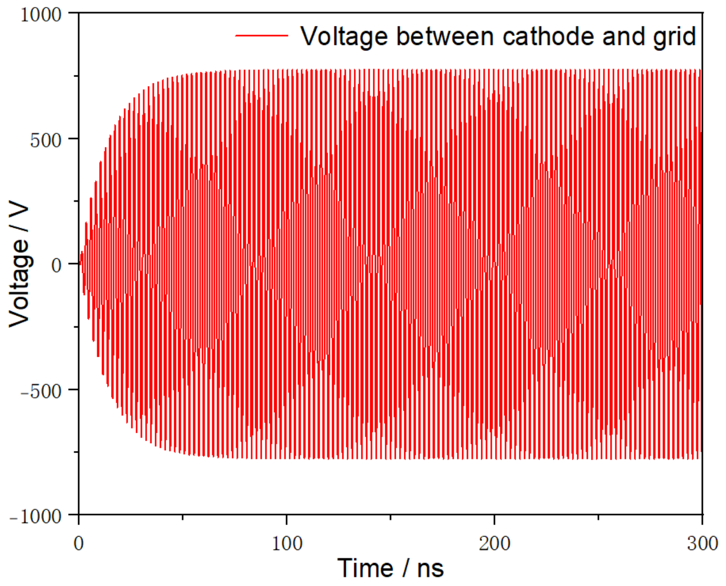


Fig.3.6 RF voltage between cathode and grid

## (2.2.1) Model of electron gun component for 434 MHz IOT

**The simulation of the electron gun is separated from the EM simulation of the input cavity . The potential of the grid can be simplified to the superposition of the DC voltage and the RF voltage.**

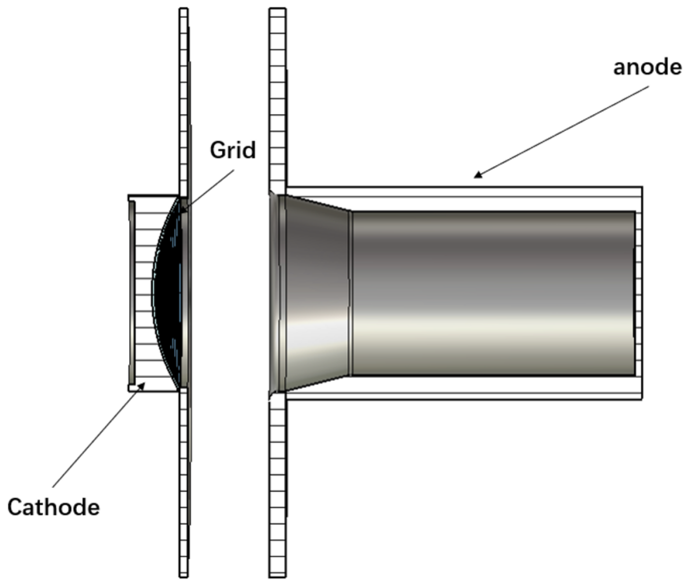


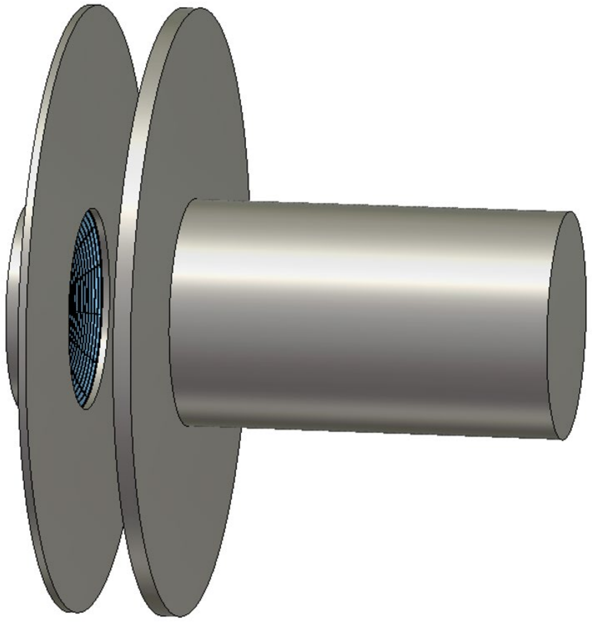

Fig.3.7 Simulation model of electron gun

## (2.2.2) Particle simulation of electron gun component for 434 MHz IOT

**Tracking Solver of CST Studio Suite was used for simulation to obtain the current emitted by the electron gun and the electron beam trajectory.**

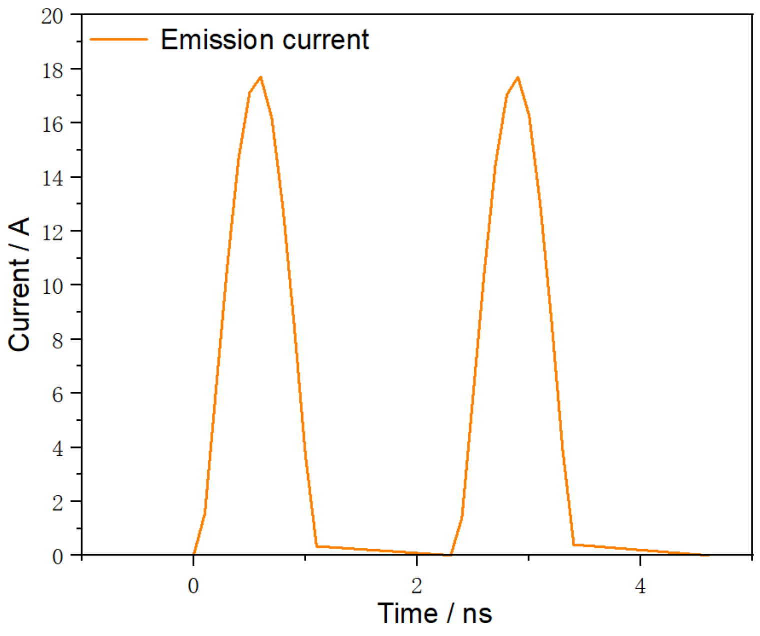


Fig.3.8 The current emitted by the electron gun

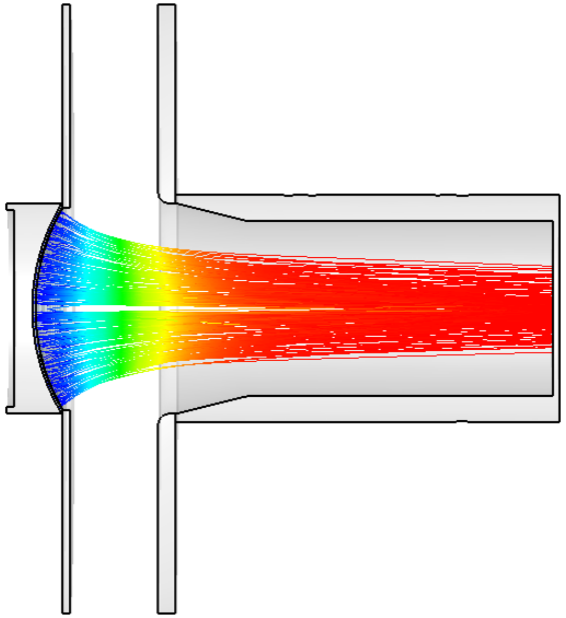

Fig.3.9 Electron beam trajectory

## (2.3.1) Model of output cavity for 434 MHz IOT

**The input cavity emits the modulated electron beam, and the energy can be extracted by a simple reentrant resonator.**

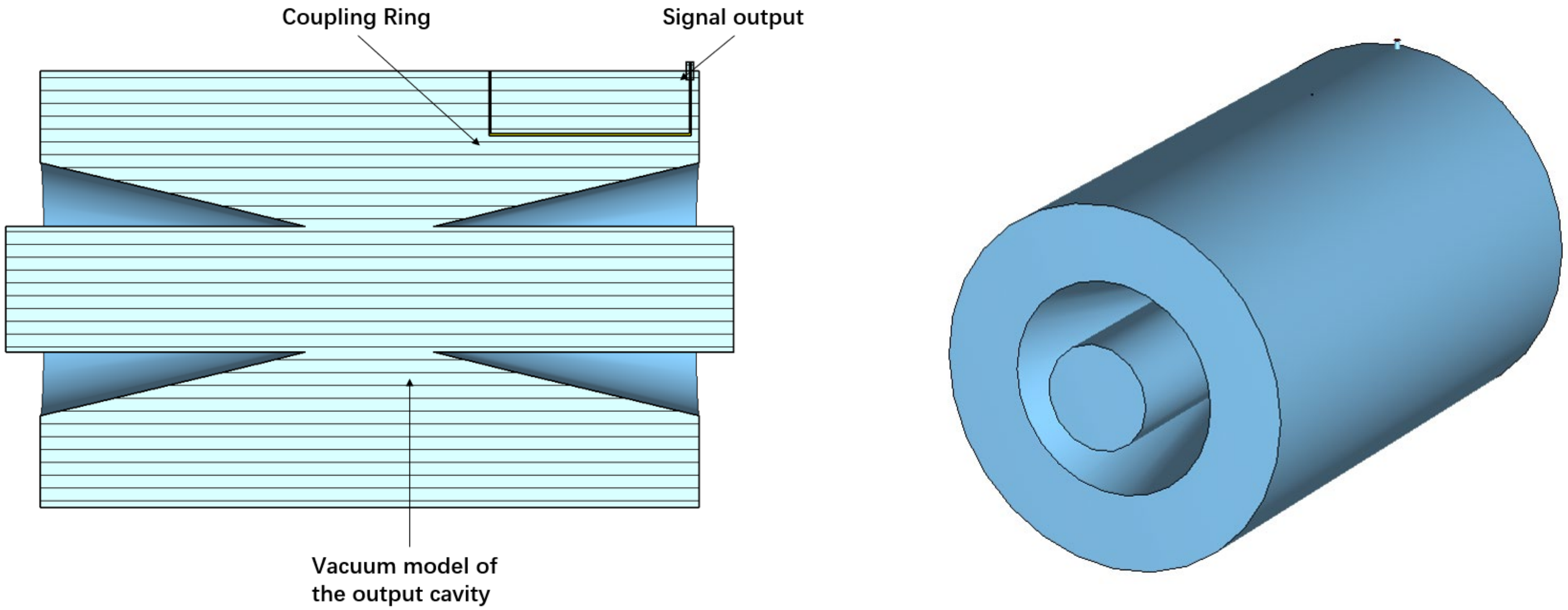


Fig.3.10 Simulation model of output cavity

## (2.3.2) Electromagnetic simulation of output cavity for 434 MHz IOT

**Electric and magnetic field distribution of the output cavity operating mode.**

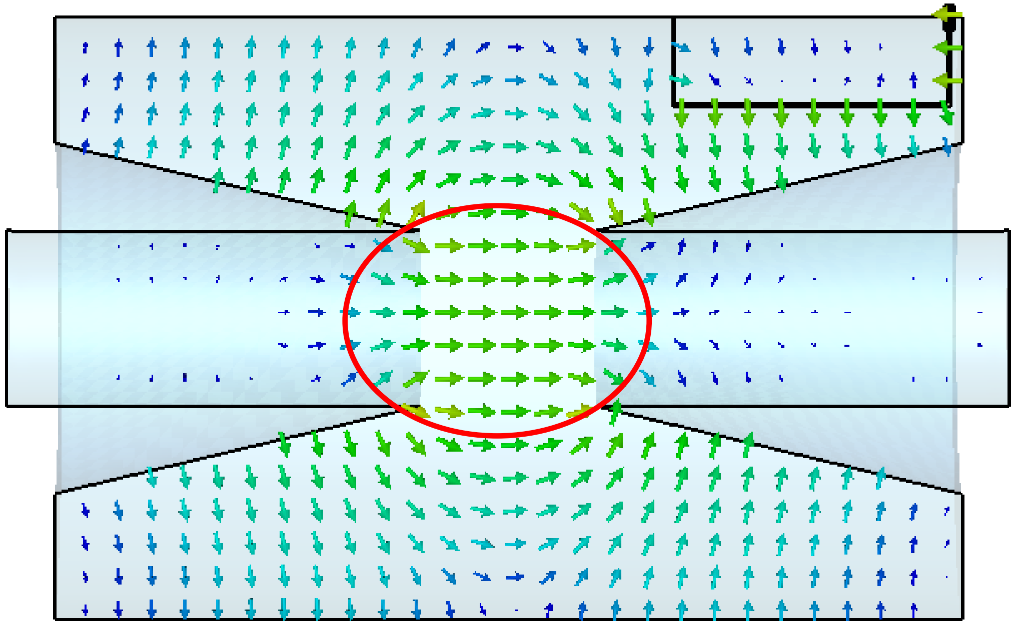

Fig.3.11 RF electric field distribution of output cavity

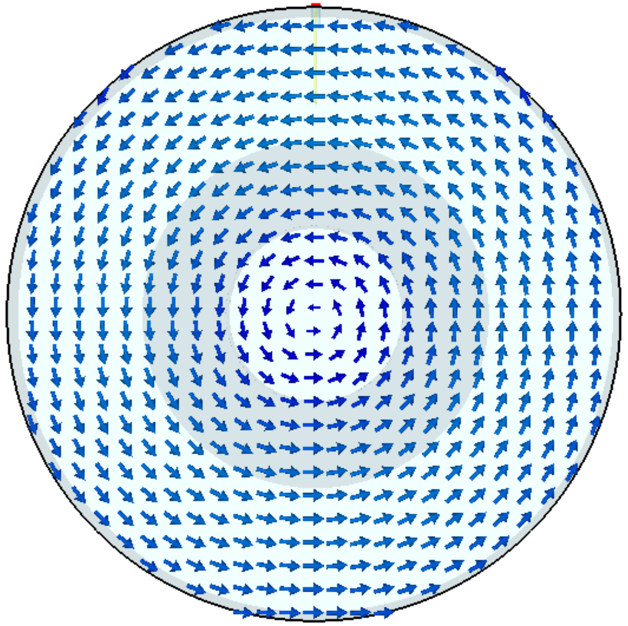

Fig.3.12 RF magnetic field distribution of the output cavity

## (2.3.3) PIC simulation of output cavity for 434 MHz IOT

**The simulation was carried out using PIC Solver of CST Studio Suite, the peak output power is 227.5 kW, efficiency of electron 47.4%.**

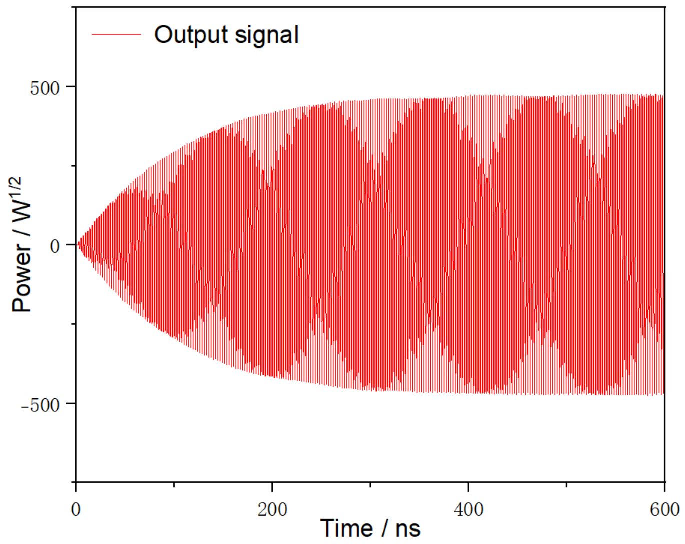


Fig.3.11 The output signal of the output cavity

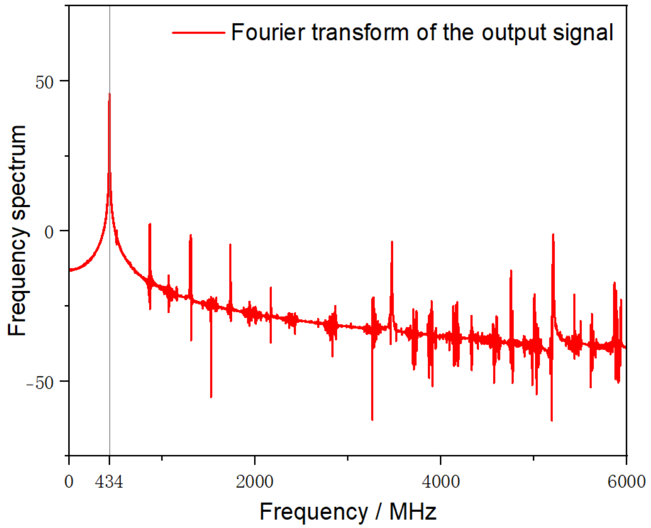


Fig.3.11 Fourier spectrum of the output signal

$$\eta = \frac{Pout/2}{\frac{Current\ anode}{4} \times Cathode\ emission\ voltage} = \frac{477^2/2}{\frac{16}{4} \times 60000} = 47.4\%$$

# Contents

**1. Introduction**

**2. Research results of 434 MHz IOT**

**3. Research results of 648 MHz IOT**

4. Research results of 915 MHz IOT

5. Summary

## (3.1.1) Model of Input cavity for 648 MHz IOT

**The 648 MHz IOT adopts a planar grid and planar cathode input cavity model.**

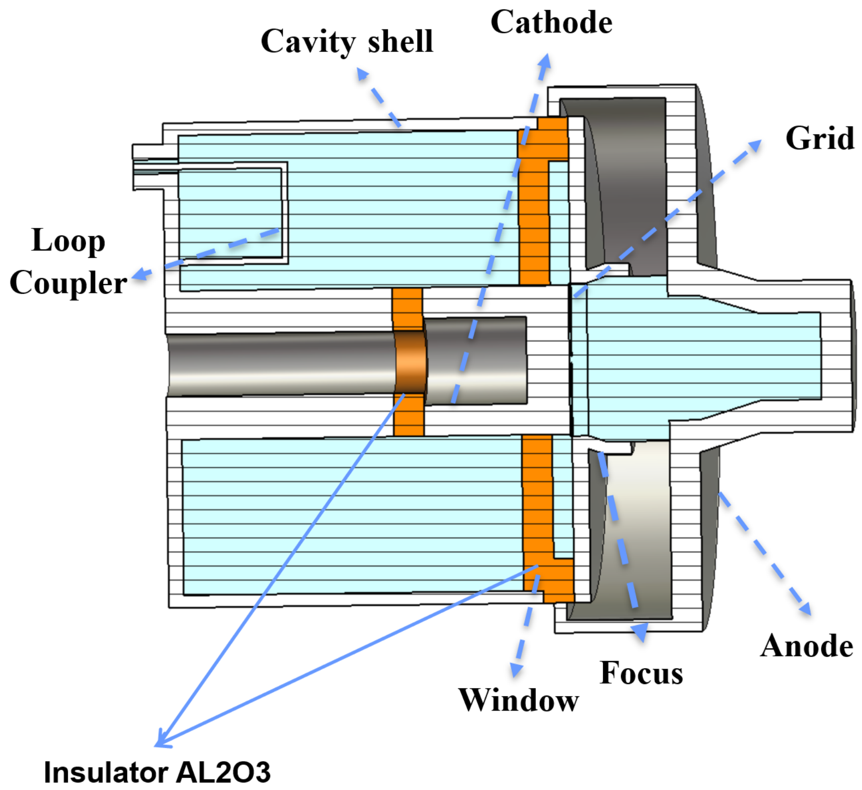


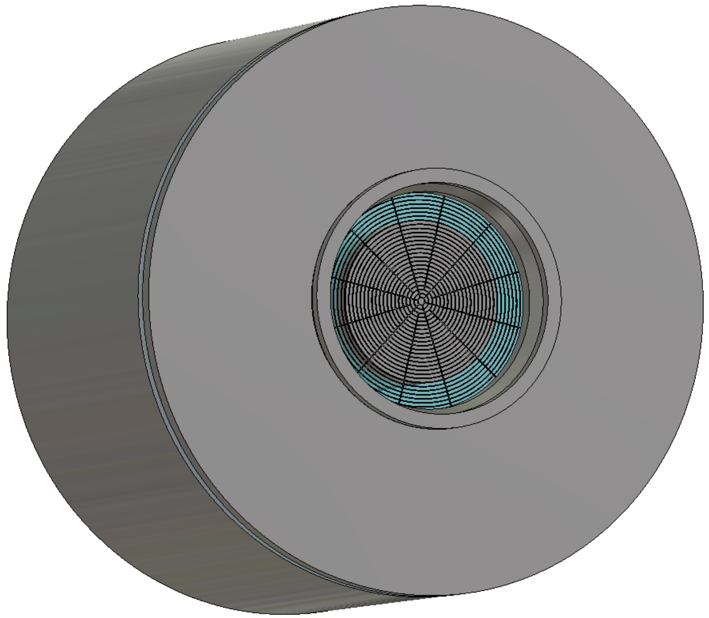

Fig.4.1 Model of  the input cavity for 648 MHz IOT

## (3.1.2) Electromagnetic simulation of Input cavity for 648 MHz IOT

**The electromagnetic simulation obtains the reflection coefficient of the input cavity, the RF voltage between the cathode and the grid and its Fourier spectrum.**

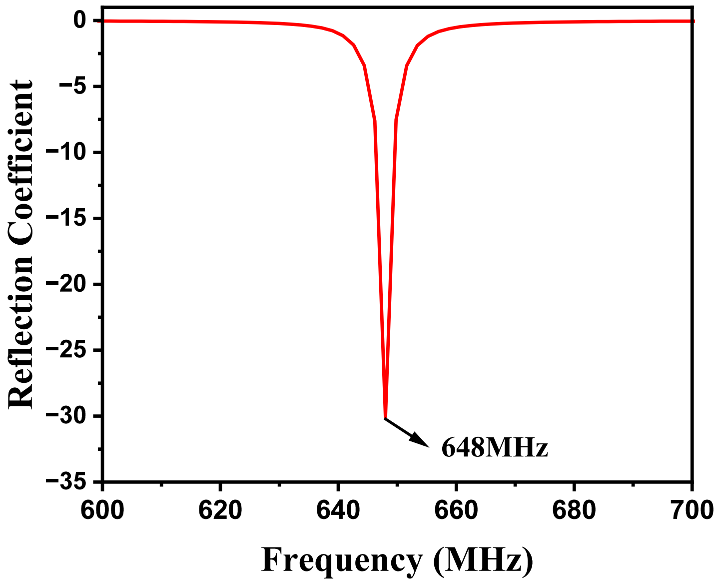


Fig.4.2 REFLECTION COEFFICIENCY

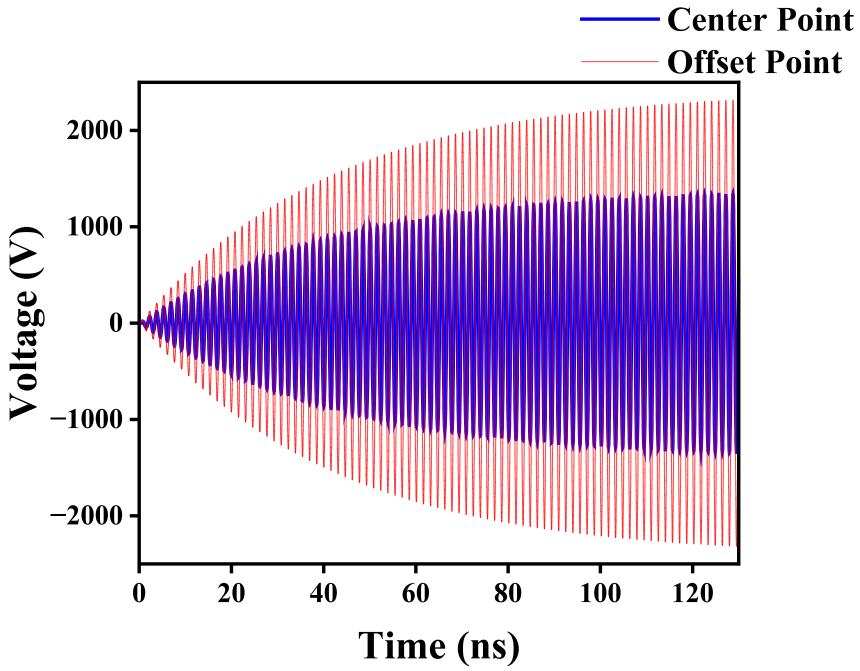


Fig.4.3 VOLTAGE MONITOR

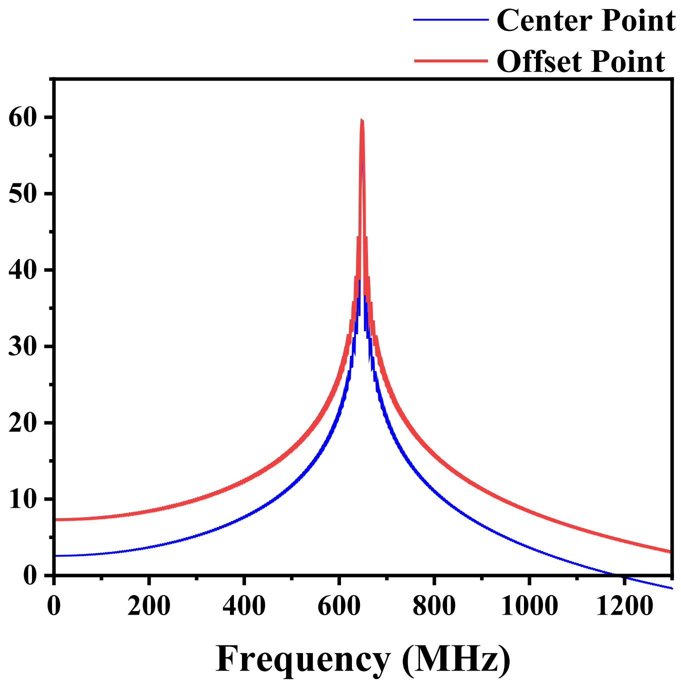


Fig.4.4 VOLTAGE MONITOR Fourier transform

## (3.2.1) Particle simulation of Input cavity for 648 MHz IOT

**The trajectory of the electron beam and the emission current of the electron gun and the intercepted current of the grid are obtained by particle simulation.**

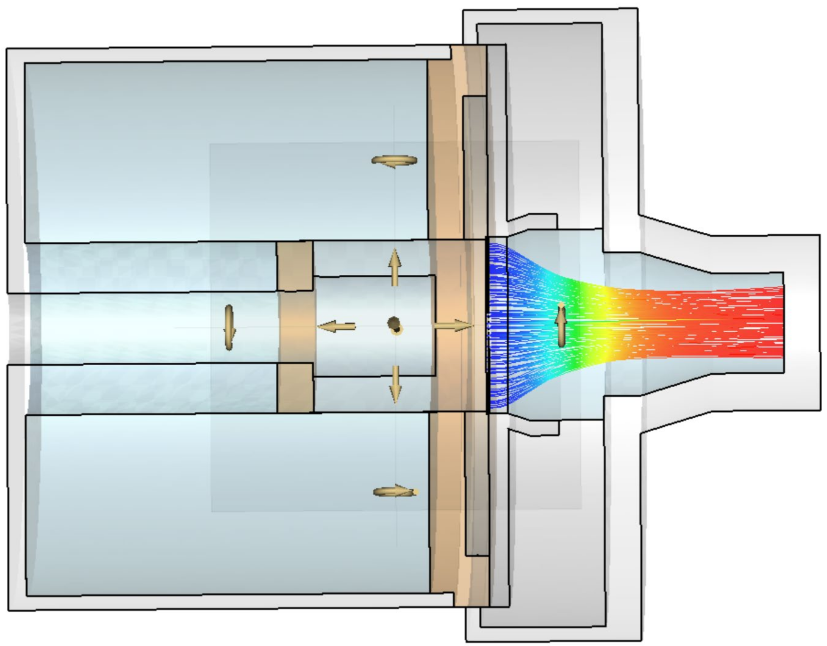

Fig.4.5 Trajectory TRACKING INFORMATION

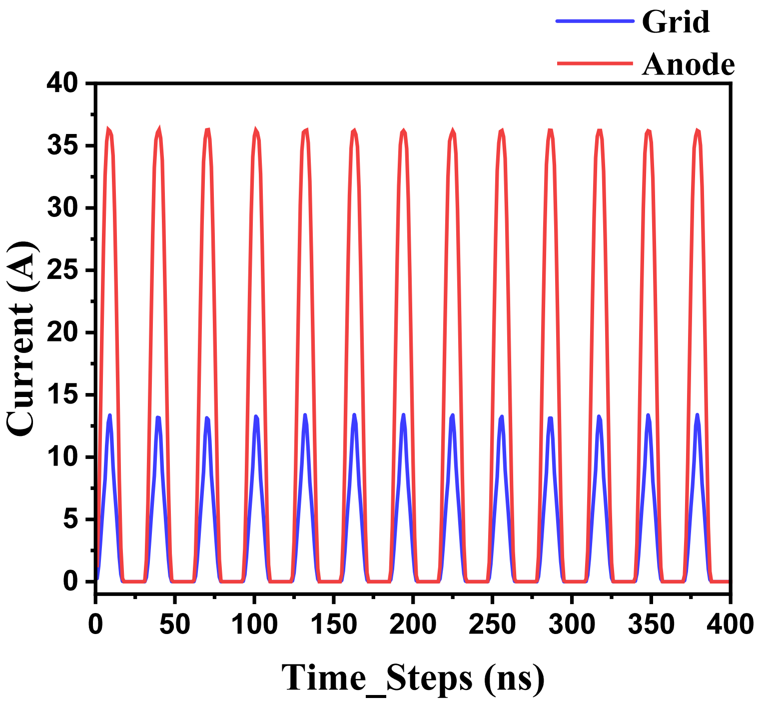


Fig.4.6 Trajectory TRACKING INFORMATION

## (3.3.1) Model of output cavity for 648 MHz IOT

**Simple modifications to the output cavity can increase the beam-wave interaction.**

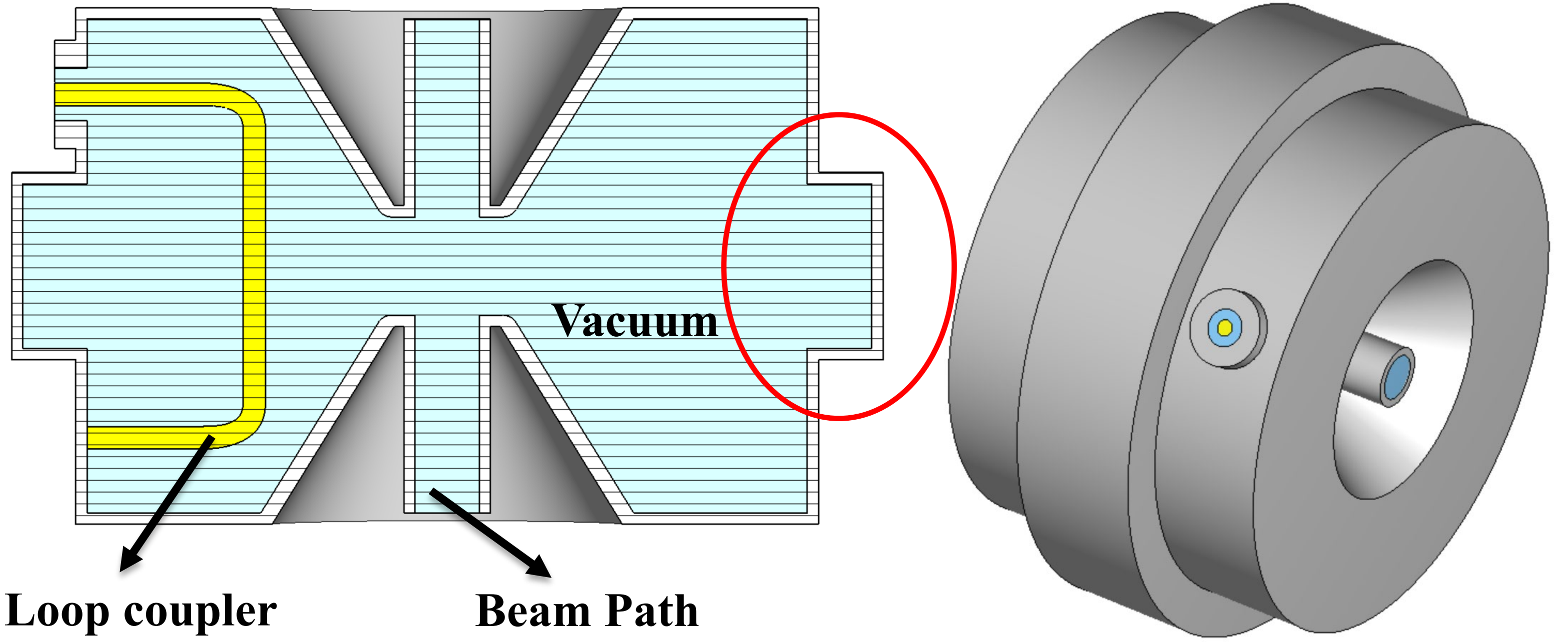


Fig.4.7 Simulation model of output cavity

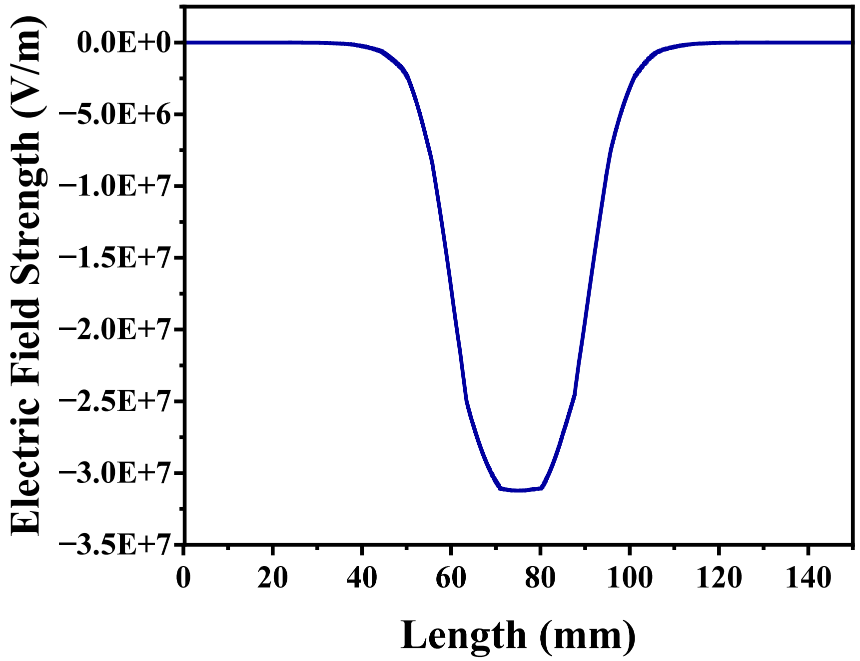


Fig.4.8 Electric field strength in the cavity

## (3.3.2) Electric field distribution of output cavity for 648 MHz IOT

**The electric field distribution of the output cavity can meet the requirements of beam-wave interaction performance.**

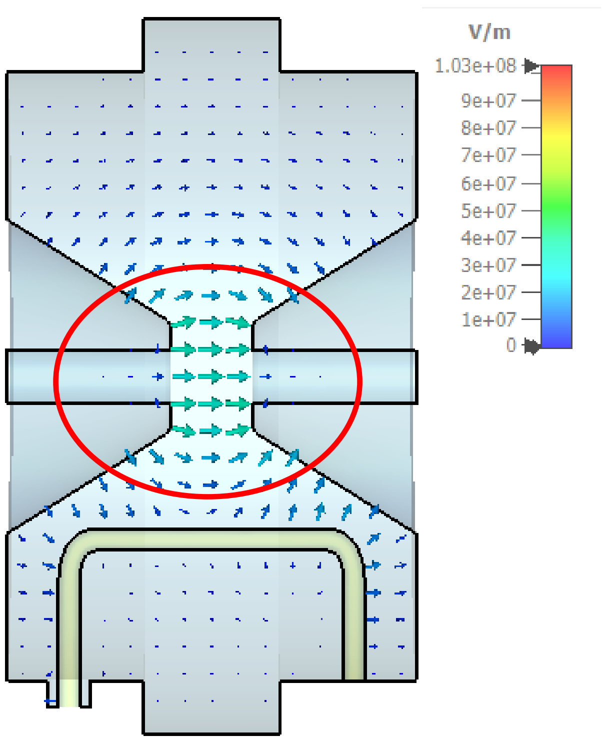


Fig.4.9 RF electric field distribution of output cavity

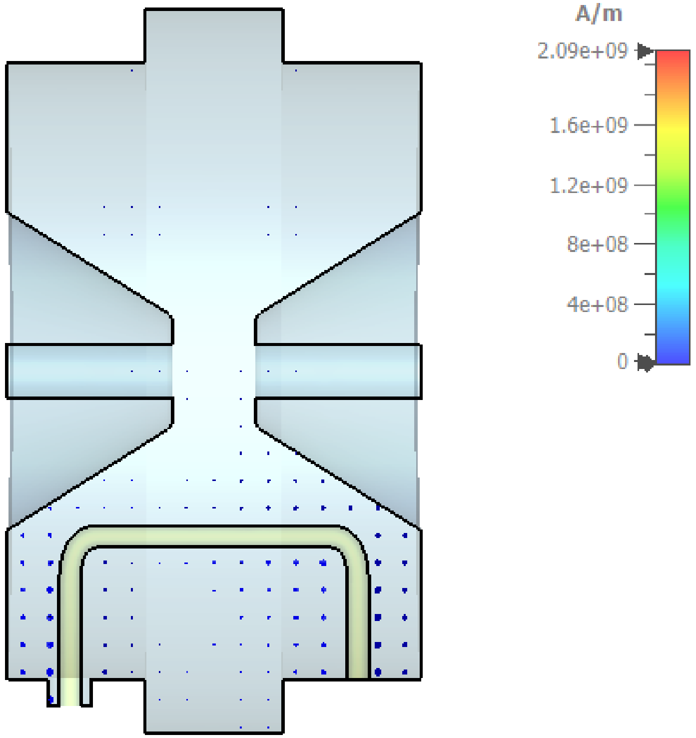


Fig.4.10 RF magnetic field distribution of the output cavity

## (3.3.3) PIC simulation of output cavity for 648 MHz IOT

**The modulated beam is used to interact with the output cavity, the output power is 908 kW, and the electronic efficiency is 71.62%.**

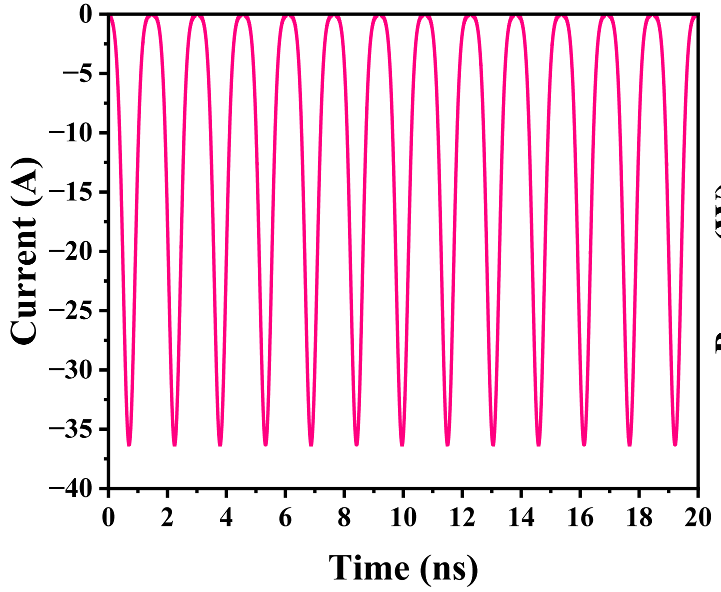


Fig.4.11 Emitted Current information

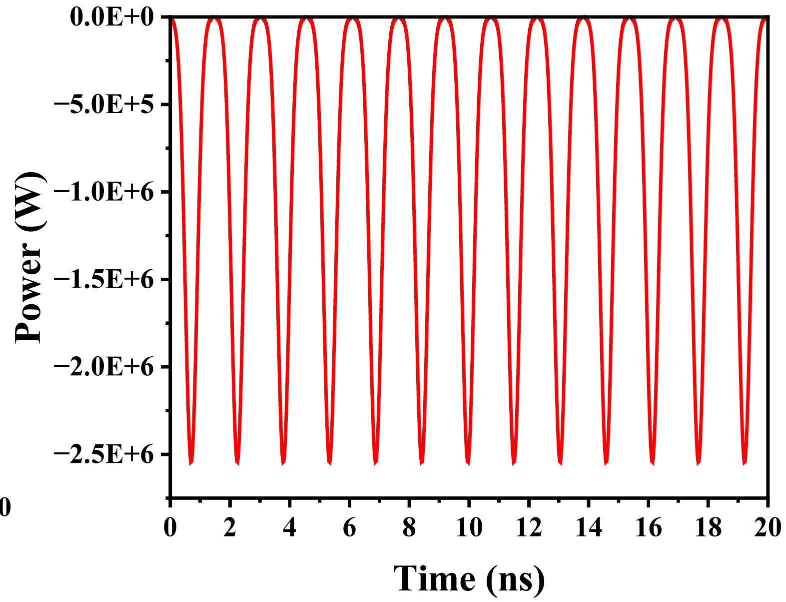


Fig.4.12 Emitted POWER information

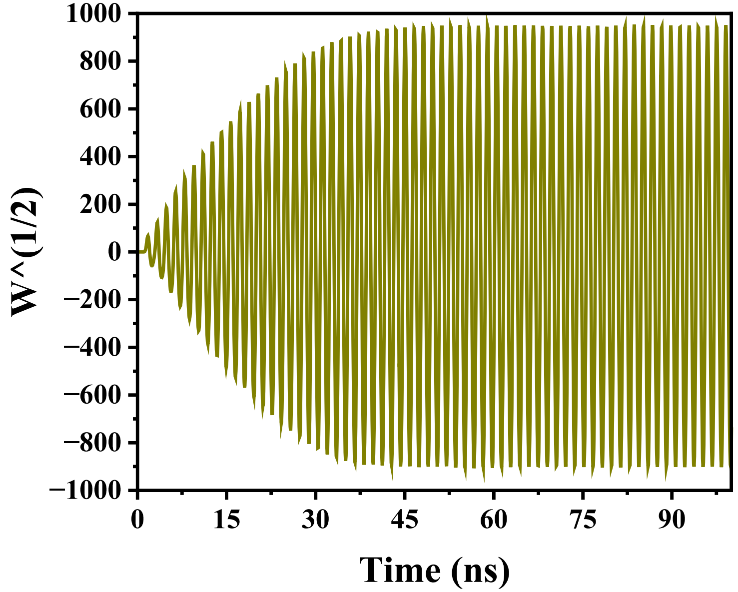


Fig.4.13 POWER OUTPUT RESULTS

$$\text{Electron } \eta = \frac{Pout/2}{\frac{Current\ anode}{4} * Cathode\ emission\ voltage} = \frac{953.94^2/2}{\frac{36.3}{4}A * 70000} = 71.62\%$$

## (3.4.1) Cold test of output cavity for 648 MHz IOT

**Screenshots of the cold test device and the cold test interface, reflection coefficient and group delay.**

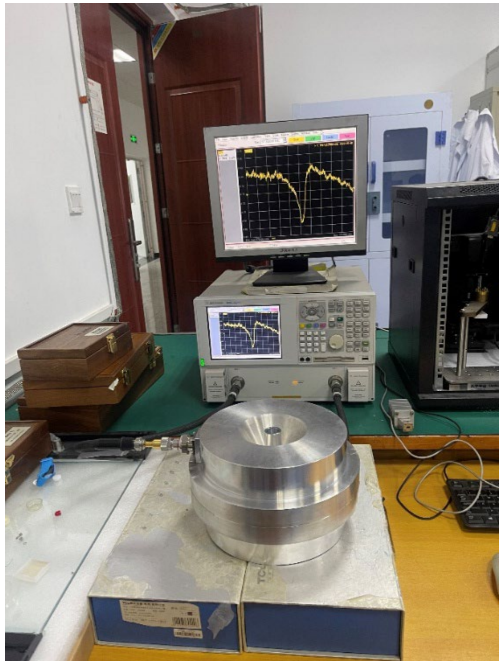

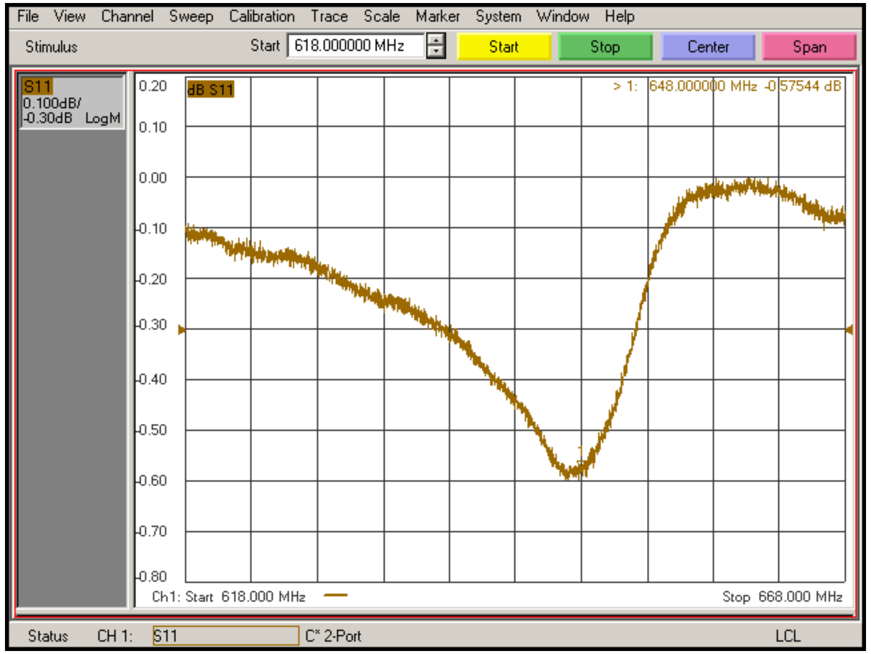


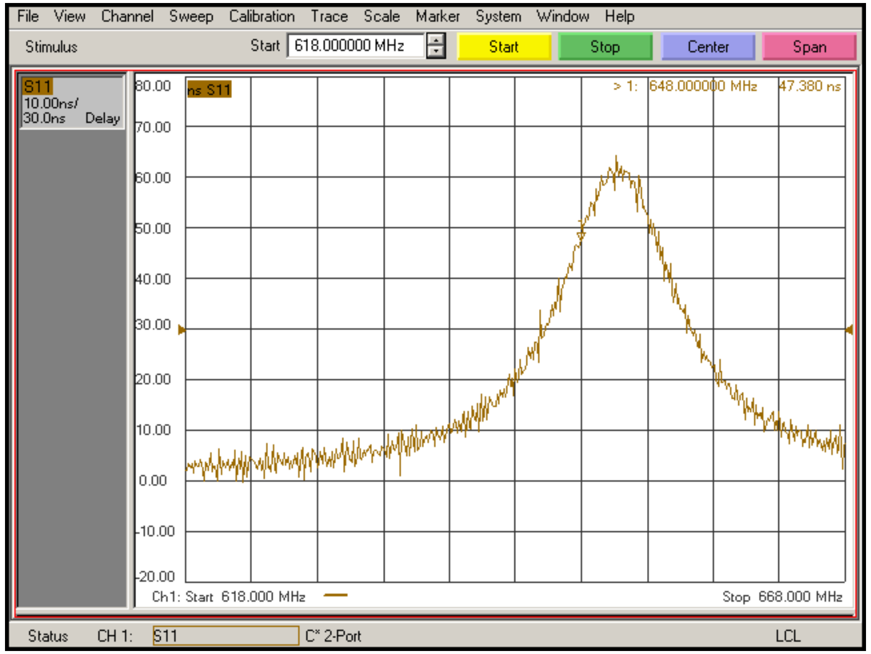


Fig.4.14 Cold testing device

Fig.4.15 Reflection coefficient and group delay obtained by cold measuring device

# (3.4.1) Cold test of output cavity for 648 MHz IOT

## Comparison of simulation results and experimental results.

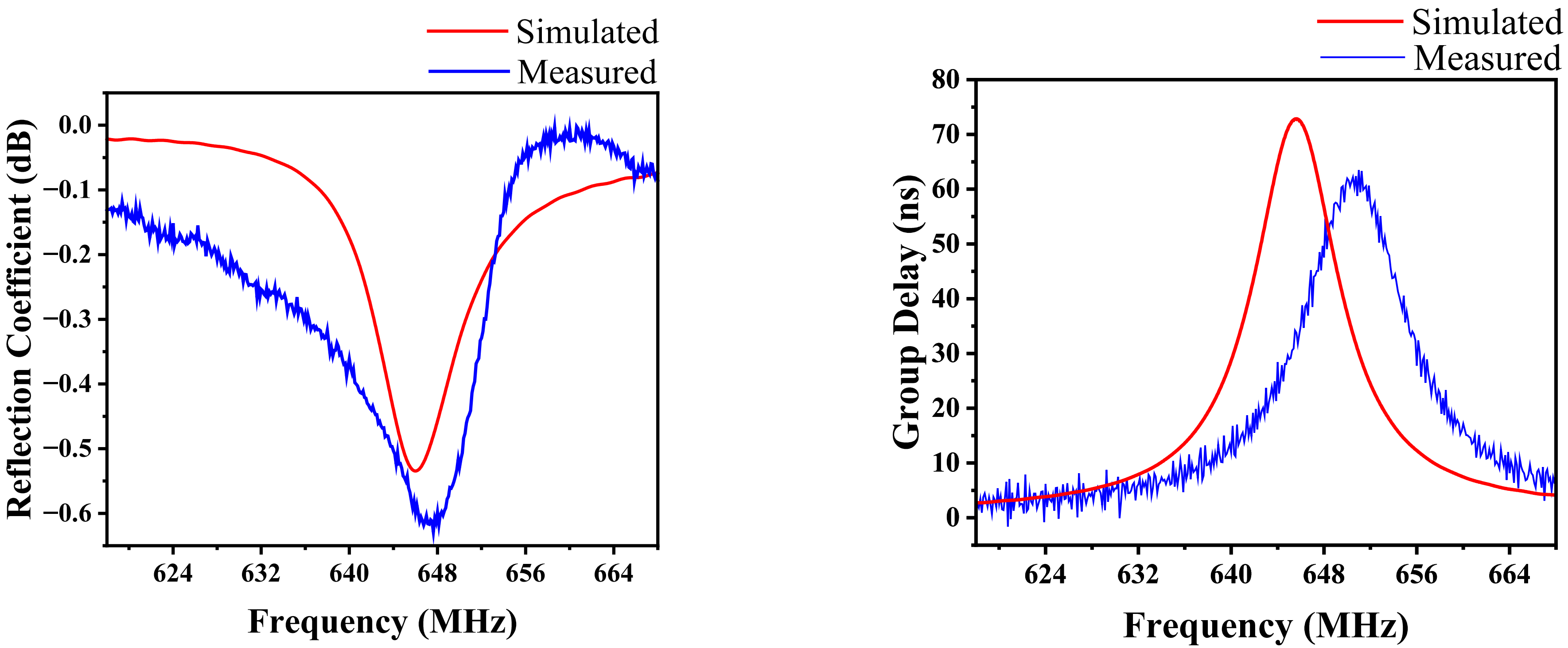


Fig.4.16 Comparison of simulation data and test data

# Contents

1. **Introduction**
2. **Research results of 434 MHz IOT**
3. **Research results of 648 MHz IOT**
4. **Research results of 915 MHz IOT**
5. Summary

## (4.1.1) Model of Input cavity- Electron gun for 915 MHz IOT

**Two types of planar grid and spherical grid are studied for 915 MHz IOT, the planar grid structure is characterized by larger emission current, and the spherical grid is characterized by better electron beam focusing.**

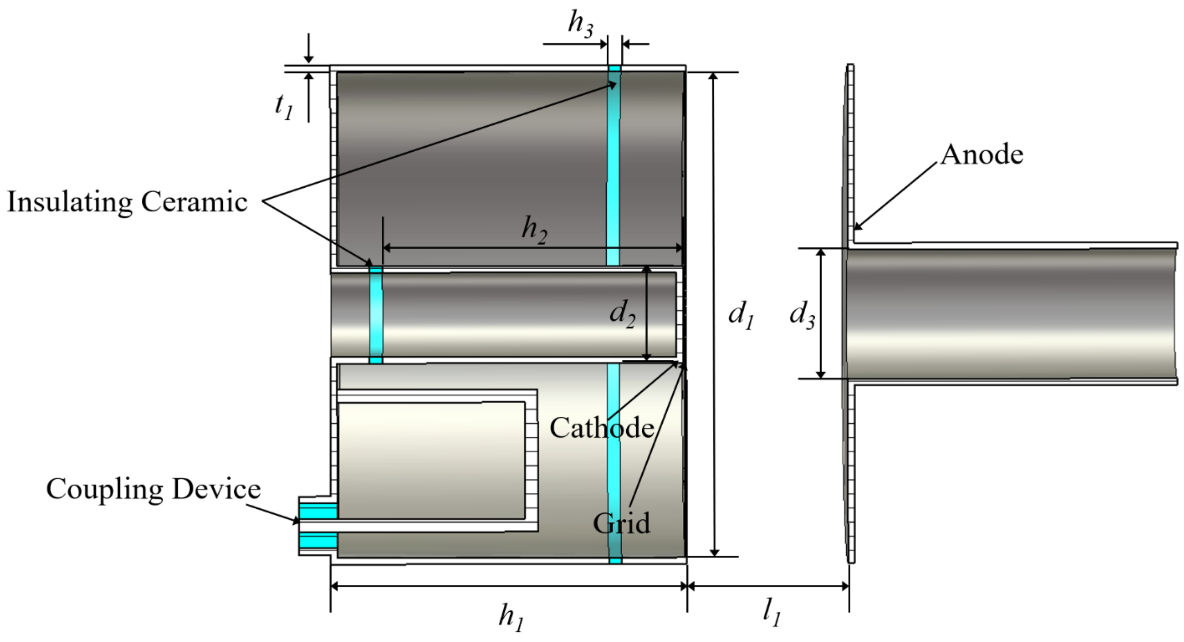


Fig.5.1 Planar Cathode Structure

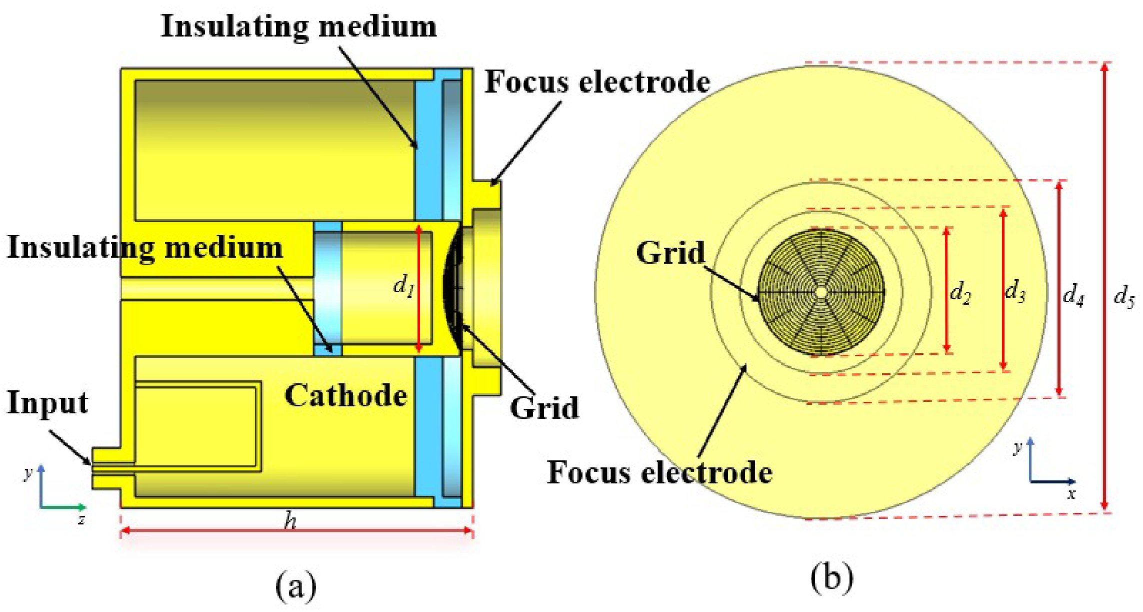


Fig.5.2 Spherical Cathode Structure

## (4.1) Electromagnetic simulation of Input cavity for 915 MHz IOT

**The electromagnetic simulation obtains the RF voltage between the cathode and the grid and its Fourier spectrum.**

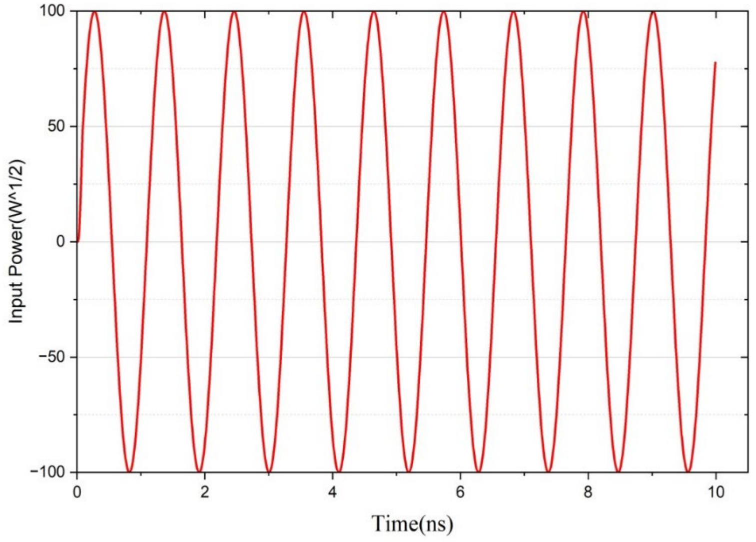


Fig.5.3 Input signal of the input cavity

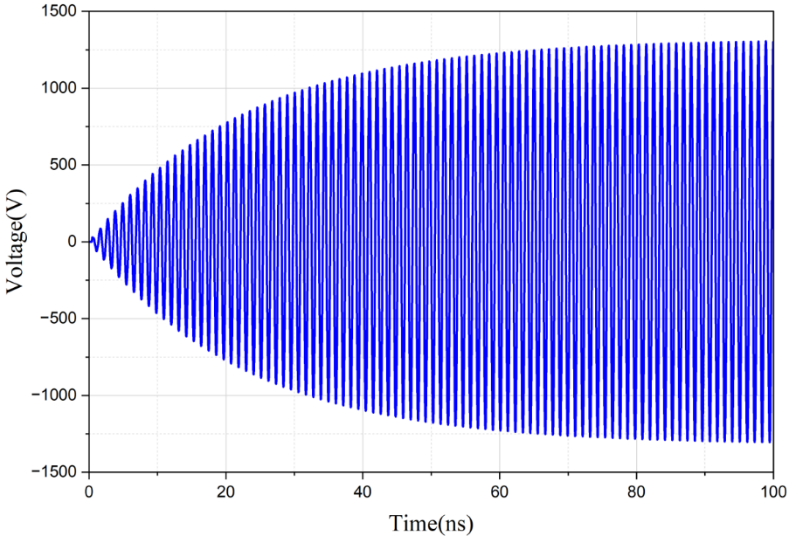


Fig.5.4 RF voltage between cathode and grid

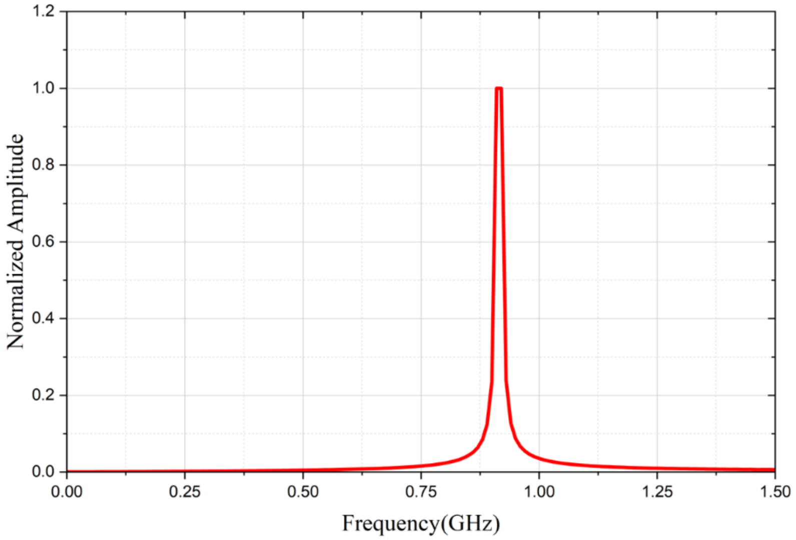


Fig.5.5 Fourier spectrum of the RF voltage between the cathode and the grid

## (4.2) Particle emission simulation of Input cavity for 915 MHz IOT

**The trajectory of the electron beam and the emission current of the electron gun and the intercepted current of the grid are obtained by particle simulation. The grid interception rate is 25.53%.**

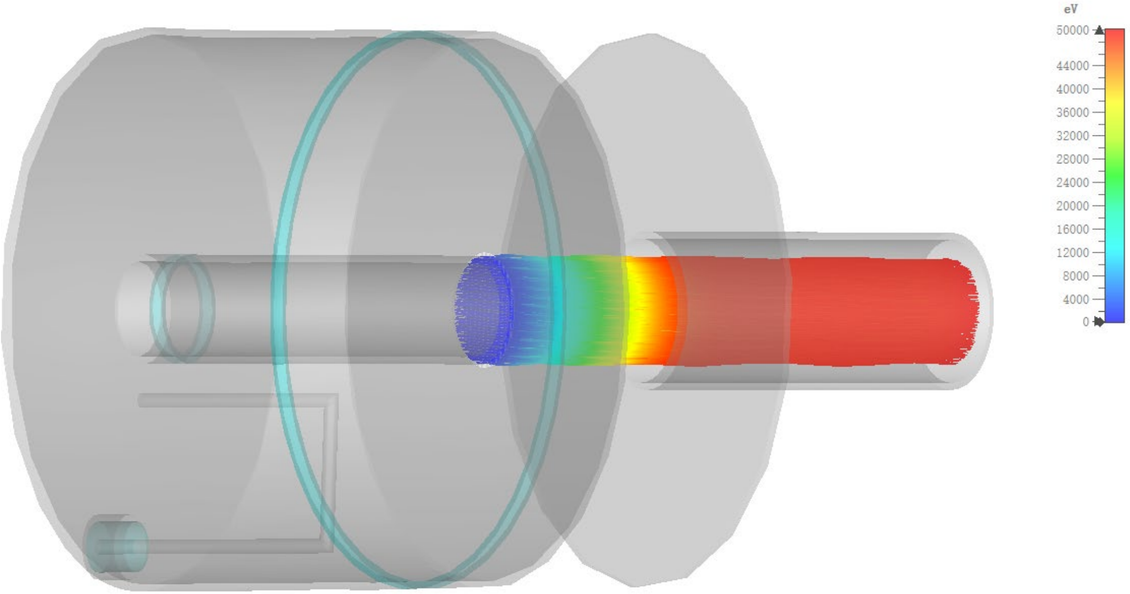


Fig.5.6 Trajectory of electrons

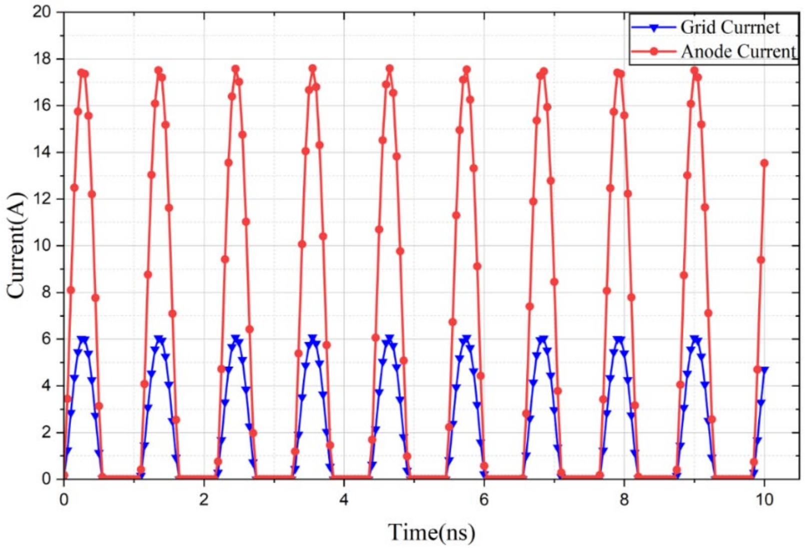


Fig.5.7 Electron gun emission current and gate interception current

## (4.2) Particle emission simulation of Input cavity for 915 MHz IOT

**After applying a periodic focusing magnetic field with a peak value of 0.2T, the electron beam is stably focused inside the drift tube.**

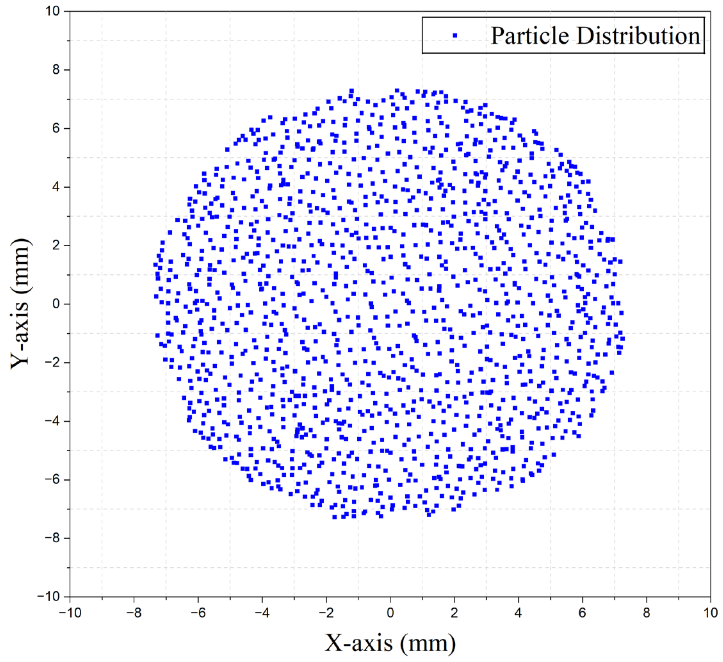


Fig.5.8 Macroparticle distribution of electron beam cross section

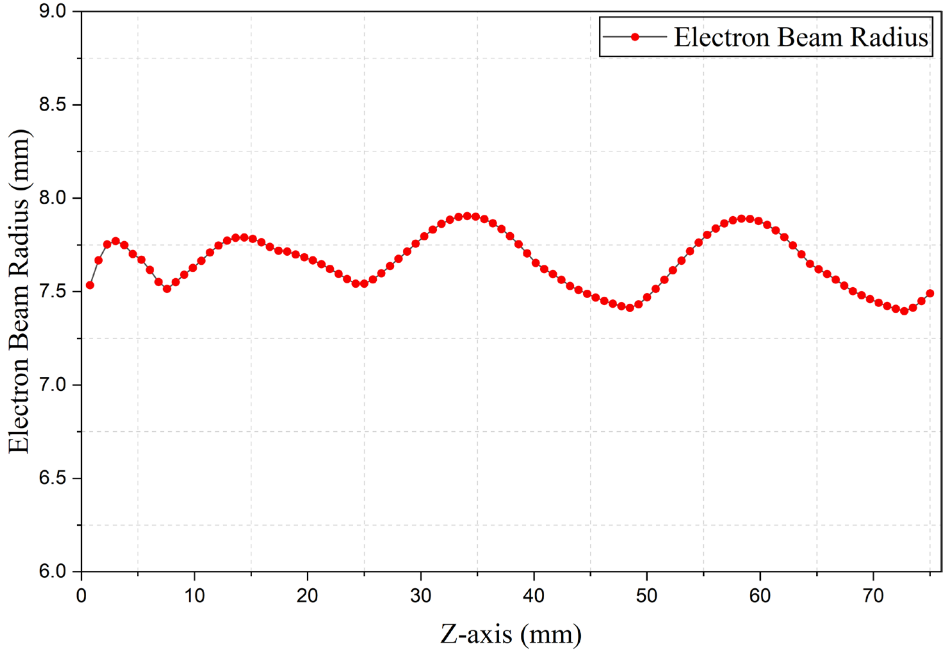


Fig.5.9 The envelope radius of the electron beam after applying the focusing magnetic field

## (4.3) PIC simulation of Input cavity for 915 MHz IOT

**The modulated beam is used to interact with the output cavity, the output power is 253 kW, and the electronic efficiency is 68.72%.**

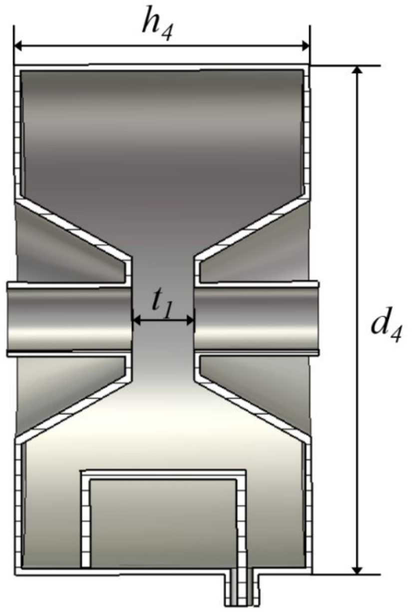


Fig.5.10 Reentrant output cavity for 915MHz IOT

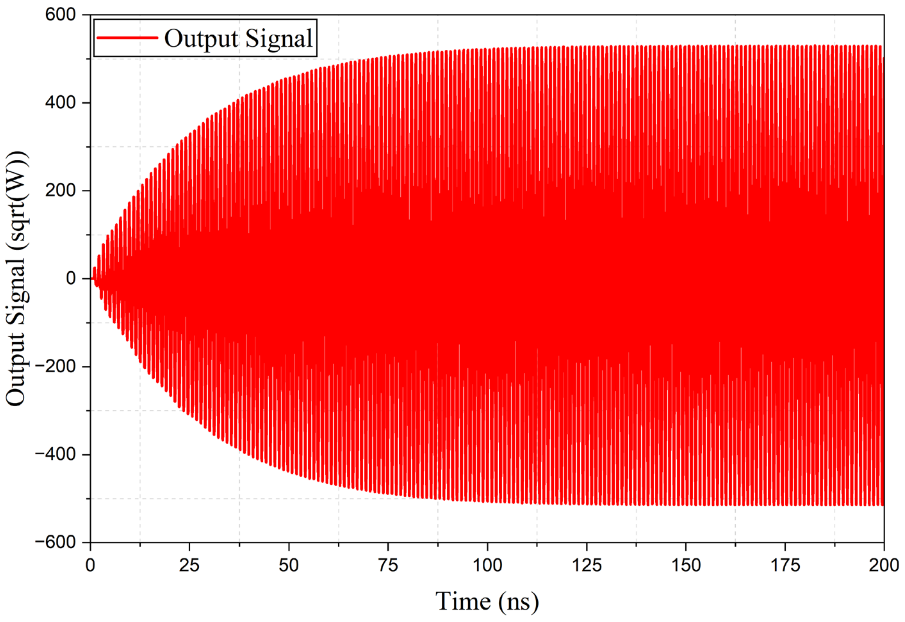


Fig.5.11 The 915MHz IOT output signal

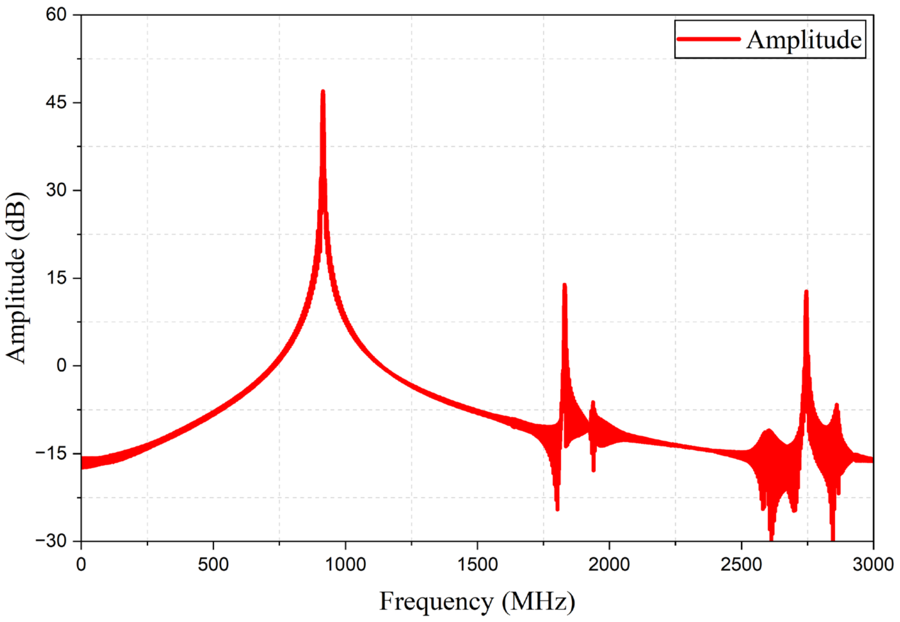


Fig.5.12 The spectrum of the 915MHz IOT output signal

## (4.4) Cold test of input cavity for 915 MHz IOT

**Processing and cold testing devices for the input cavity, reflection coefficient and group delay.**

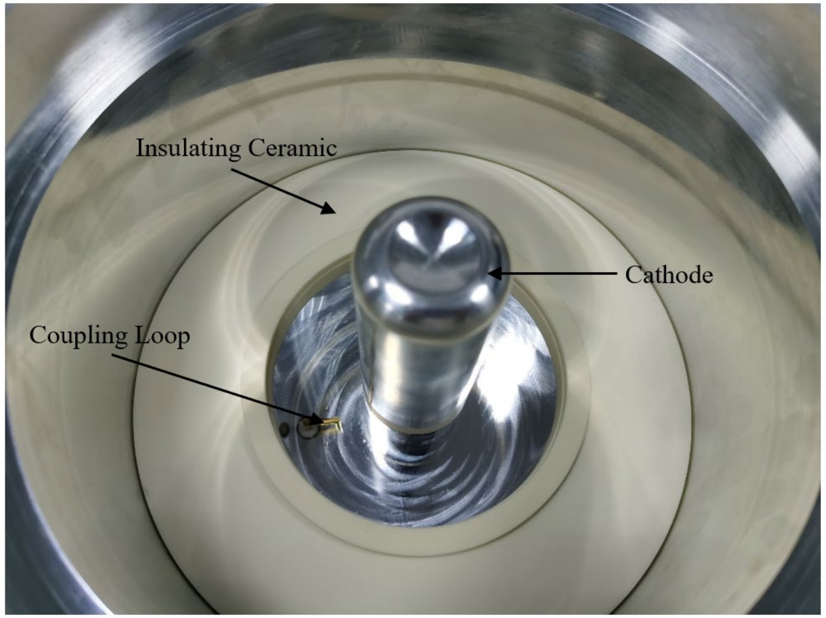


Fig.5.13 Processing and assembly of the input cavity

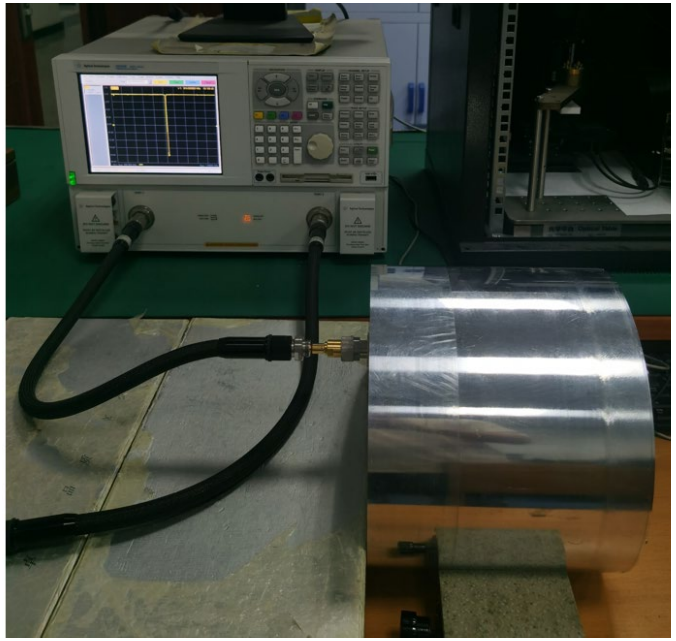

Fig.5.14 The reflection coefficient obtained from the input cavity cold test

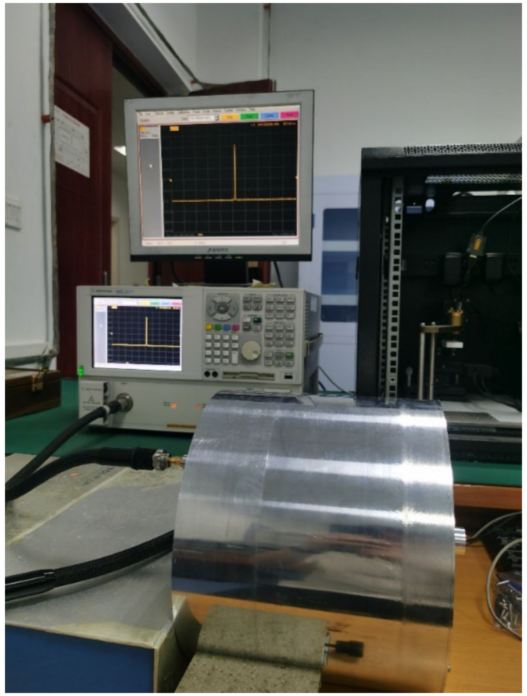

Fig.5.15 The group delay obtained from the input cavity cold test

## (4.4) Cold test of output cavity for 915 MHz IOT

**Processing and cold testing devices for the output cavity, Smith chart.**

(a)

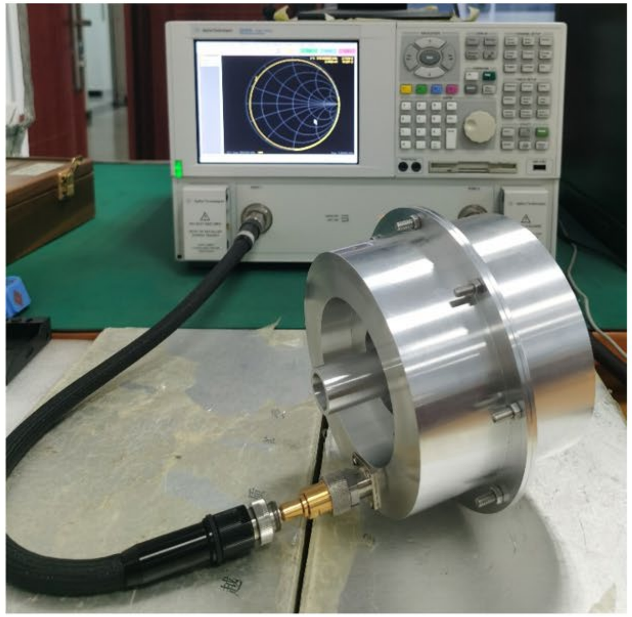

(b)

Fig.5.16 Processing of the output cavity and Smith chart testing

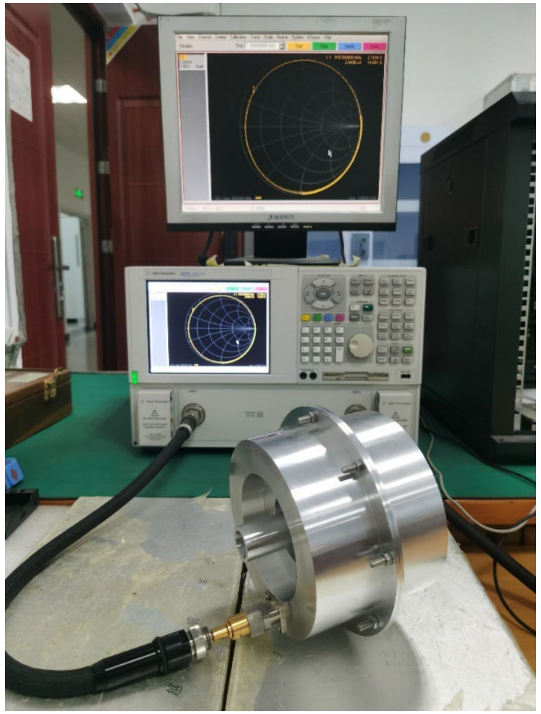

Fig.5.16 Output cavity cold test device

# Contents

# 5. Summary

## 1. Research results of 434 MHz IOT

| Spherical grid | Output Power: 227.5 kW | Electron efficiency: 47.4% |
|---|---|---|

## 2. Research results of 648 MHz IOT

| Planar grid | Output cavity cold test | Output Power: 908 kW | Electron efficiency: 71.62% |
|---|---|---|---|

## 3. Research results of 915 MHz IOT

| Planar grid & Spherical grid | Input and Output cavity cold test | Output Power: 253 kW | Electron efficiency: 68.72% |
|---|---|---|---|

# Thank you for your attention!

ybgong@uestc.edu.cn

School of ESE,UESTC

Chengdu, China